Electronic Theses and Dissertations   Graduate School

2012

A Comparative Study of Segmented Tungsten Rod Penetration Into a Thick Steel Target Plate

Michael Bryant Presnell

A COMPARATIVE STUDY OF SEGMENTED TUNGSTEN ROD PENETRATION INTO A
THICK STEEL TARGET PLATE

A Thesis

presented in partial fulfillment of requirements

for the degree of Master of Engineering Science

in the Department of Mechanical Engineering

The University of Mississippi

by

MICHAEL B. PRESNELL

May 2012

ABSTRACT

This thesis presents results from computational simulations of tungsten alloy segmented rod projectiles (SRP) penetrating an RHA semi-infinite target plate at high velocities. Penetration experimental data show improved penetration efficiency by the segmented projectiles when compared to monolithic (single solid rod) projectiles. For SRP with an aspect ratio (L/D) = 1/8, a loss in penetration efficiency was seen upon successive segment impacts. A numerical simulation impacting tungsten heavy alloy against RHA 4340 steel was performed using the Lagrangian finite element code EPIC 2006. The impact configuration that was modeled consisted of eight successive collinear impacts of discs measured 2mm in thickness and 16mm in diameter and travelling at 2.6km/sec. Normandia and Lee, using an Eulerian finite element code (AUTODYN), performed numerical simulations of the same configuration of the segmented rod penetration into RHA plates. Their results were compared and contrasted with those of EPIC 2006. Additionally the role of back-flowing ejecta was examined and found to perforate incoming segments. In an effort to increase penetration performance, an alternate SRP design was tested. This design implemented a hole in the center through which back-flowing ejecta would be allowed to flow unimpeded.

DEDICATION

This thesis would not have been possible without the tireless optimism and expert guidance of my thesis adviser Dr. Rajendran. I am also extremely thankful for the emotional support of Carrie LeMay and my parents.

LIST OF ABBREVIATIONS AND SYMBOLS

$\sigma_{ij,j}$ Stress tensor

ϵ_{ij} Strain tensor

$u_{i,j}$ Displacement tensor

ρ Density

f_i Body Force

$\ddot{u}_i$ Acceleration

c Speed of Sound

K Bulk Modulus

G Shear Modulus

E Elastic Modulus

ν Poisson's Ratio

Y_0 Projectile Strength

R_t Target Strength

α Non-dimensional parameter which describes the extent of the plastic zone

U Shock Velocity

u Particle Velocity

P Pressure

C_0 Bulk Speed of Sound

C_1 Static Yield Stress

C_2 Hardening Coefficient

C_3 Strain Rate Coefficient

$\dot{\varepsilon}^N$ Dimensionless strain rate normalizing factor

M Softening Exponent

N Hardening Exponent

L/D Projectile aspect ratio (length divided by diameter)

P/L Penetration efficiency (depth of penetration divided by projectile length)

SRP Segment Rod Projectile

LRP Long Rod Projectile

DOP Depth of Penetration

AOA Angle of attack (measure of segment pitch and yaw)

RHA Rolled Homogenous Armor (a 4340 steel)

D_1/D_{seg} Ratio of diameter of crater created by impact of first segment to diameter of segment

Δ Distance from crater bottom at which segment is completely converted to meshless particles

ACKNOWLEDGMENTS

TABLE OF CONTENTS

LIST OF TABLES

LIST OF FIGURES

Chapter 1

INTRODUCTION

The main objective of this thesis is to fundamentally understand the unsteady penetration of a segmented tungsten rod at high velocities into a thick steel target through high resolution computational simulations. However, to acquire an understanding of unsteady penetration it is first necessary to understand the steady state penetration process. When a body of arbitrary mass strikes another at an arbitrary velocity, compressive stress waves are initiated and propagated into both objects. Material response to wave propagation is characterized by the velocity of impact, the sound wave velocity, density, and other mechanical properties of both impactor and target materials. In addition, the geometry of the striker and target, and the impact configuration (obliquity of impact, presence of projectile spin, etc) can greatly modify the complexity of the penetration process.

At low velocities, below the Hugoniot Elastic Limit (HEL) of both the projectile and target materials, elastic stress waves are generated from the impact surface. These waves will eventually reflect back from lateral boundaries according to the boundary conditions. However, above a certain threshold velocity (above HEL), plastic stress waves will propagate following the elastic waves (elastic precursor). At impact velocity levels above the HEL, the

stresses imposed on both penetrator and target materials are significantly greater than their yield

strengths, therefore, the deformation and material failure behaviors are significantly influenced

by material strength. In addition to equation of state (EOS), an accurate constitutive description

(strength model) is essential in modeling the wave propagation characteristics.

The problem of impact mechanics begins at the same place all mechanics problems do: at

their governing equations. The governing equations for elastic wave propagation problems are

the force equilibrium equation (or equation of motion), Hooke's Law, and the strain-

displacement relation:

$$\sigma_{ij,j} + \rho f_i = \rho \ddot{u}_i \ (1)$$

$$\sigma_{ij} = \lambda \epsilon_{kk} \delta_{ij} + 2\mu \epsilon_{ij} \ (2)$$

$$\epsilon_{ij} = \frac{1}{2}(u_{i,j} + u_{j,i}) \ (3)$$

σ_{ij} and ϵ_{ij} are the stress and strain components, λ and μ are Lame's constants, ρ is the material

density, and u_i are displacements The variable f_i represents the body forces on the continuum.

Combined they form the displacement equation of motion: the form of the classical equation of

wave motion:

$$\frac{\partial^2 \Psi}{\partial t^2} = c^2 \frac{\partial^2 \Psi}{\delta x_i \delta x_i} \ (4)$$

For elastic wave propagation, the parameter c depends on whether target undergoes one-

dimensional stress or strain. Equations (5) and (6) describe the characteristic elastic wave

velocity for one-dimensional stress condition and one-dimensional strain condition, respectively.

$$c_e = \sqrt{\frac{E}{\rho}} \quad (5)$$

$$c_L = \sqrt{\frac{K + 4G/3}{\rho}} \quad (6)$$

K and G are bulk and shear modulus, respectively. These equations are not adequate to describe the wave propagation, deformation, and material failure when a long rod projectile penetrates into thick metallic targets at velocities well above HEL. The stress – strain states are multiaxial and plastic waves are generated due to material yielding. The wave speeds become function of particle velocity (or pressure levels). The projectile penetration problems become highly nonlinear and require advanced computing capabilities. With the absence of such compuer capabilities during 60s and 70s, several analytical models were developed to describe penetration of cylinder shaped rigid projectiles into thick metallic targets. For instance, Tate [1] first performed an analysis of this penetration configuration for a one dimensional case, while a thorough review and discussion of the models commonly employed for this type of penetration was made by Anderson and Walker [2]. A wide range of data is available on the penetration of heavy alloy long rods into thick targets having planar surfaces, and much effort has been put into computational and analytical modeling of the penetration process with generally acceptable results. A comprehensive collection of penetration data for a planar target surface is available in the penetration mechanics database report compiled by Anderson et al. [3]. Rajendran [4] presented a computational analysis of penetration of tungsten alloy rods into a shallow-cavity steel target to understand the effects of ejecta from the cavity surfaces on penetration efficiency of the projectile.

The wave propagation, deformation, and failure processes related to the penetration of long rods into thick targets are highly complex, especially at very high striker or impact velocities. The process is under such conditions is quasi-hydrodynamic. The highly distorted projectile material due to large plastic deformation is basically ejected from the penetrator/target interface, in conjunction with failed target material. Many papers discussing this system are available; Solutions to the problem of projectile penetration into thick targets according to Zukas [5], be divided into three different categories: purely empirical, simplified analytical, and numerical models. The expense of performing experiments and scarcity of existing experimental data for unsteady rod penetration does not allow for direct empirical modeling but certain related data may be used for comparison. No experimental data exists on the topic of multiple collinear segments for different L/D (projectile length, L divided by the projectile diameter, D). Therefore, the solution must be approached from a numerical perspective whilst using analytical modeling which utilize certain assumptions as a check on the numerical solution. With the advent of advanced hydrocodes (shock wave propagation-based finite element or volume codes which can be Lagrangian or Eulerian) and computer capabilities, it is now possible to estimate depth of penetration into targets by a variety of metallic projectiles using high resolution discretization techniques.

During the past two decades, researchers working on the armor and anti-armor studies reported that compared to a single solid tungsten rod penetration into a thick steel target, a segmented tungsten rod of same mass penetrates more efficiently at very high velocities above 1 km/sec. Most results for segmented rod penetration problems have been reported in obscure or proprietary technical reports. Unfortunately, there are hardly any DOP data available in open literature. Most of the design concepts and enhanced understanding related to unsteady

4

penetration of segmented rods could be accomplished using high resolution hydrocodes simulations.

The main objective of this thesis is to study and understand the penetration mechanisms of segmented rods into a thick steel target at high velocities. For this purpose, three distinctly different projectile configurations were considered in the present work. A Lagrangian code called EPIC [6] was employed in the computational simulations. The first configuration was a solid rod of length to diameter (L/D) ratio of 1, the second was an eight-solid disks (segmented rod), and the third was an 8-segment rod with alternate solid and annular disks. The single solid rod penetration was simulated to establish the depth of penetration of a base line case for comparison with alternate projectiles with the same mass of the single long rod. The DOP results for the second configuration from EPIC code simulations were directly compared with the results reported by Normandia and Lee [7] who performed simulations using the AUTODYN [8] (Eulerian) code. Additional EPIC [6] simulations examined reasons for the differences between DOPs determined from EPIC and AUTODYN. In the EPIC simulations, a phenomenon called "back flowing ejecta" was identified and the various effects of ejecta on the penetration efficiency of the segmented rods were studied. The rest of the work examined the influence of several parameters such as projectile velocity, aspect ratio of the projectile, failure criterion, and type of failure on the DOP

1.1 Background

In armor and other protection system applications, it is essential to develop a fundamental understanding of the penetration process of a projectile into these systems at high velocities. While experiments provide time-resolved DOP data, high resolution computational simulation often provide an in-depth understanding of the penetration process. With the advent of computing capabilities, high resolution finite element simulations enable design analysis of protective systems, such as improved body and vehicular armors, impact resistant airplane canopies, nuclear reactor shrouds, and other structures. However, the study of penetration mechanics often employ simplified analytical models [9,10] under mostly steady state penetration conditions. The analytical modeling of a long rod projectile (LRP) penetration into semi-infinite targets is based on a one-dimensional state of stress at the impact point. The stress-strain relation can be expressed as:

$$\sigma_1 = \frac{E}{1-2v}\varepsilon_1 \quad (7)$$

Typically, kinetic energy (K.E) projectiles, such as a solid tungsten LRP will often have Length/Diameter (L/D) ratio of 10 or more. However, a segmented rod projectile will have very small L/D ratio (<<1). The stress state during the initial penetration phase (a few microseconds) is more closed to one-dimensional strain for the segmented rod penetrator. For one-dimensional strain the stress and strain relations in the principal coordinates use the following relationships:

$$\varepsilon_1 = \varepsilon_1^e + \varepsilon_1^p \quad (8)$$

$$\varepsilon_2 = \varepsilon_2^e + \varepsilon_2^p \quad (9)$$

$$\varepsilon_3 = \varepsilon_3^e + \varepsilon_3^p \quad (10)$$

$$\varepsilon_2 = \varepsilon_3 = 0 \quad (11)$$

Where, $\varepsilon_1, \varepsilon_2,$ and ε_3 are total principal strains; the superscripts "e" and "p" represent elastic and plastic strain components respectively.

$$\varepsilon_2^p = -\varepsilon_2^e \quad (12a)$$

$$\varepsilon_3^p = -\varepsilon_3^e \quad (12b)$$

Introducing the incompressibility condition allows the total one dimensional strain in terms of elastic strain:

$$\varepsilon_1^p + \varepsilon_2^p + \varepsilon_3^p = 0 \quad (13)$$

$$\varepsilon_1^p = -\varepsilon_2^p - \varepsilon_3^p = -2\varepsilon_2^p \quad (14)$$

$$\varepsilon_1^p = 2\varepsilon_2^e \quad (15)$$

$$\varepsilon_1 = \varepsilon_1^e + \varepsilon_1^p = \varepsilon_1^e + 2\varepsilon_2^e \quad (16)$$

The elastic stress-strain relations may now be determined:

$$\varepsilon_1^e = \frac{\sigma_1}{E} - \frac{v}{E}(\sigma_2 + \sigma_3) = \frac{\sigma_1}{E} - \frac{2v}{E}\sigma_2 \quad (17a)$$

$$\varepsilon_2^e = \frac{\sigma_2}{E} - \frac{v}{E}(\sigma_1 + \sigma_3) = \frac{(1-v)}{E}\sigma_2 - \frac{v}{E}\sigma_1 \quad (17b)$$

7

$$\varepsilon_3^e = \frac{\sigma_1}{E} - \frac{v}{E}(\sigma_1 + \sigma_2) = \frac{(1-v)}{E}\sigma_3 - \frac{v}{E}\sigma_1 \text{ (17c)}$$

A combination of equations (16) and (17) yields:

$$\varepsilon_1 = \frac{\sigma_1(1-2v)}{E} + \frac{2\sigma_2(1-2v)}{E} \text{ (18)}$$

By using the von Mises yield condition, equation (19), and combining it with equation (18) produces:

$$\sigma_1 - \sigma_2 = Y_0 \text{ (19)}$$

$$\sigma_1 = \frac{E}{3(1-2v)}\varepsilon_1 + \frac{2}{3}Y_0 = K\varepsilon_1 + \frac{2Y_0}{3} \text{ (20)}$$

When the disc thickness is much smaller compared to the diameter, the central region of the target remains under uniaxial strain condition for a longer period of time compared to a rod of L/D ratio 1. This is important as it means that the projectile's kinetic energy is not laterally dispersed and is thus more efficiently used during impact. It is this concept of more efficient use of impact energy which forms the basis of improved penetration depths in segmented rods.

The current state of research in the area of unsteady penetration processes is incomplete. A few reports and articles that are available in the open literature certainly support the basic trends related to projectile penetration efficiency and crater morphology in segmented rod penetration process. However, there is hardly any detailed finding or discussion on the underlying mechanisms, such as the back flowing ejecta.

The concept of segmented penetrators is that of creating more penetration with the same amount of mass launched at a target. As early as 1956, Eichelberger [11] suggested that spaced

8

metallic jets (often used as an analog to rods impacting at high velocity) could improve penetration by up to 40%. Since then, researchers [12-27] have demonstrated, through a mixture of numerical simulations and experiments, an increase in penetration efficiency (penetration per unit length of penetrator) with SRP over their monolithic equivalents (equal diameter and mass).

Current SRP literature generally pertains to either SRP with short-rod segments ($1 \leq L/D \leq 4$) or disc-like segments ($1/4 \leq L/D \leq 1/32$). Nearly all of the experimental literature involves short-rod segments while a fair amount of computational literature is dedicated to disk-like segments. This interest in short rods is borne out of practical launch considerations. In a direct ballistic loading method (projectile launched at target), these segments are less likely to yaw upon impact. Experimental configurations include those which utilize a low-impedance metal tube (such as aluminum) with brittle material spacers (Figure 1.1). Others utilize a thin threaded tube to join the segments into a coaxial train (Figure 1.2). These systems are effective at launching segment with a short-rod type of aspect ratio but are limited in usefulness that they can only produce a limited amount of total penetration.

Segmented projectiles penetrate by means of an unsteady process. Both Tate [1] and Walker and Anderson [28] developed engineering models based on equation (21) which is a modified Bernoulli's equation. Since this equation is one dimensional and a penetration event must be considered in at least two dimensions, variables must be created to account for the projectile and target's resistance in one dimension to the penetration process. This is the role of the parameters Y_p and R_t (the projectile and the target respectively). Tate's analytical expressions focused on optimizing spacing between segments. A problem in this model was some discrepancies seen during the transient beginning and end of penetration [1]. This problem
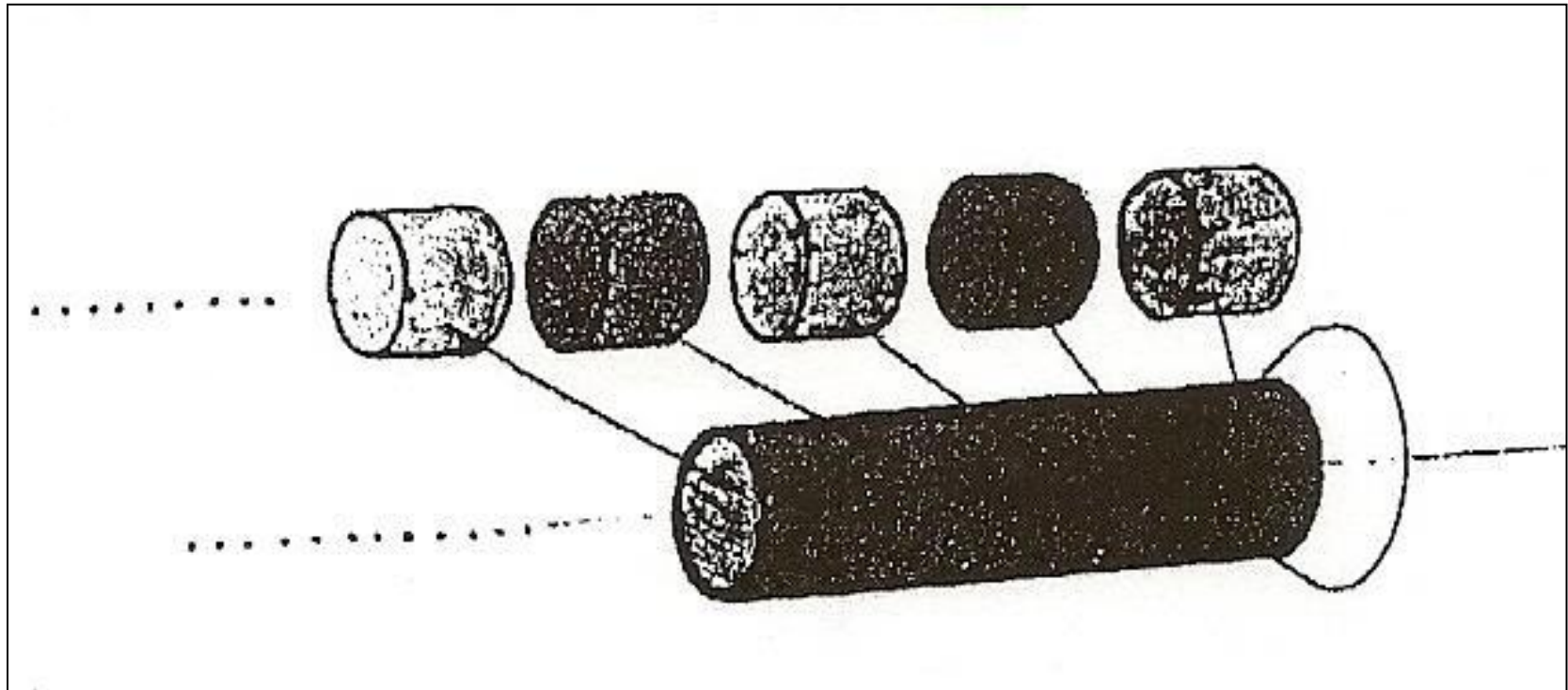
Figure 1.1. SRP with tungsten alloy segments and plastic spacers slip-fit inside aluminum sleeve [23]
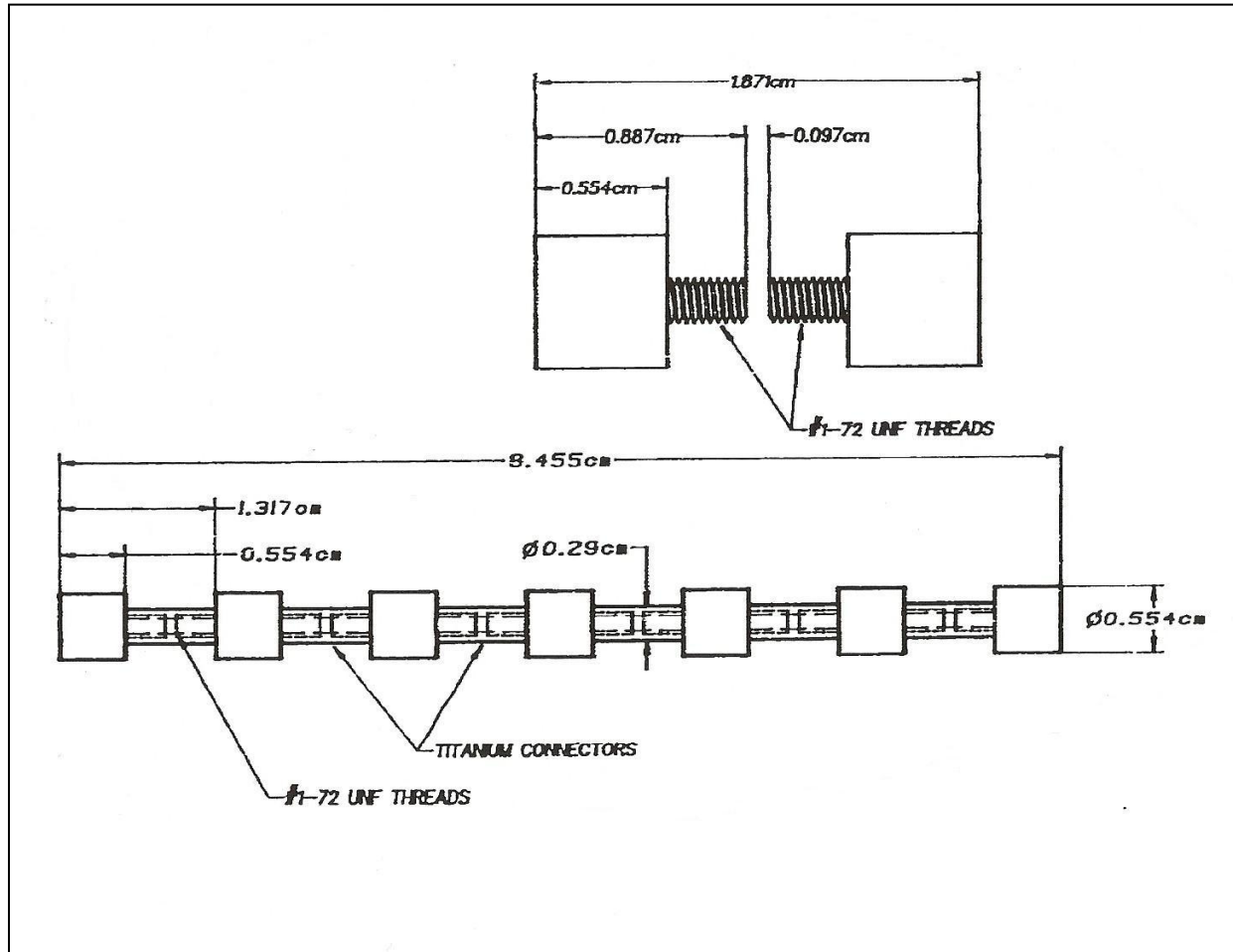
Figure 1.2. SRP with tungsten segments threaded into titanium connectors. [14]

was addressed by Walker and Anderson [28] by formulating time variation of the target material strengths.

$$\frac{1}{2} \rho_p (v-u)^2 + Y_p = \frac{1}{2} \rho_t u^2 + R_t \quad (21)$$

The R_t parameter does not represent the "real" flow strength of the target material and it is a pseudo strength parameter introduced by Tate [1]. Using its values, the target resistance to projectile penetration can be quantified and various impact configurations can be compared through this parameter. Partom, Anderson, and Orphal [29] reported their investigation of this parameter through computer simulations of a tungsten long rod penetration into a semi-infinite steel target at various impact velocities. The main purpose of their computational study was to validate the dependence of R_t on target strength and projectile impact velocity. The final conclusion was that the R_t parameter cannot be defined due to the absence of a steady state penetration process; the eventual interactions between the penetrating projectile and the eroded projectile materials makes projectile penetration unsteady. Therefore, use of the R_t parameter to characterize target penetration resistance is not possible in the SRP configuration.

As mentioned before, spacing of the segments is key, maladjustment of which will result in less than optimal performance. If the subsequent segment arrives too early, it will "clash" with the current segment and will lose significant energy penetrating through the current segment before it reaches the target. Additionally, there is a point when backward-flowing ejecta interferes with the incoming segment. Segment spacing has not always been a concern as practical considerations (such as a limit on overall package length) cause some experiment designers to use a less than ideal spacing.

Regarding ejecta resulting from impact, Hohler and Stilp [20] experimentally observed that such interference reaches a maximum for segment spacing of two diameters. It should be noted that in their experiments, the segment L/D was 1 and shrinking the aspect ratio will undoubtedly alter the spacing at which such interference occurs. However, this observation does hold merit as the velocity regimes of the paper and the current work are similar. Hunkler [26] as well as Weirauch and Wollman [23] mention significant loss in penetration performance due to ejecta interference while de Rosset [24] echoes a more commonly found opinion that the effects are negligible. While there is a divided consensus, it should be remembered this has been formed on data involving short rod segments and not disk-like segments.

Segment penetration efficiencies, defined as DOP divided by penetrator thickness, have been shown by simulation and experimental results to vary with segment-aspect ratio. Figure 1.3 (from the work of Normandia and Lee [7]) illustrates leveling of penetration efficiencies which becomes less pronounced as the aspect ratio (L/D) goes to unity. The simulations reported by Tolman et al [30] give efficiencies which possess an odd oscillatory penetration efficiency (Figure 1.4). This is to be expected as the simulation results of Normandia et al [7] are based on perfectly normal impacts by each of the segments onto to the target surface whereas the work of Tolman et al [30] is experimental and so includes irregularities such as angular deflection of the segment caused by its interaction with the delivery system. Segment yaw and pitch is collectively termed angle of attack (AOA) and creates an irregular crater profile which in turn leads to non-uniform penetration processes by subsequent segment impacts. Tolman et al [30] cited a maximum yaw of 1.62 degrees and minimum yaw of 1.12 degrees in the four datasets produced.
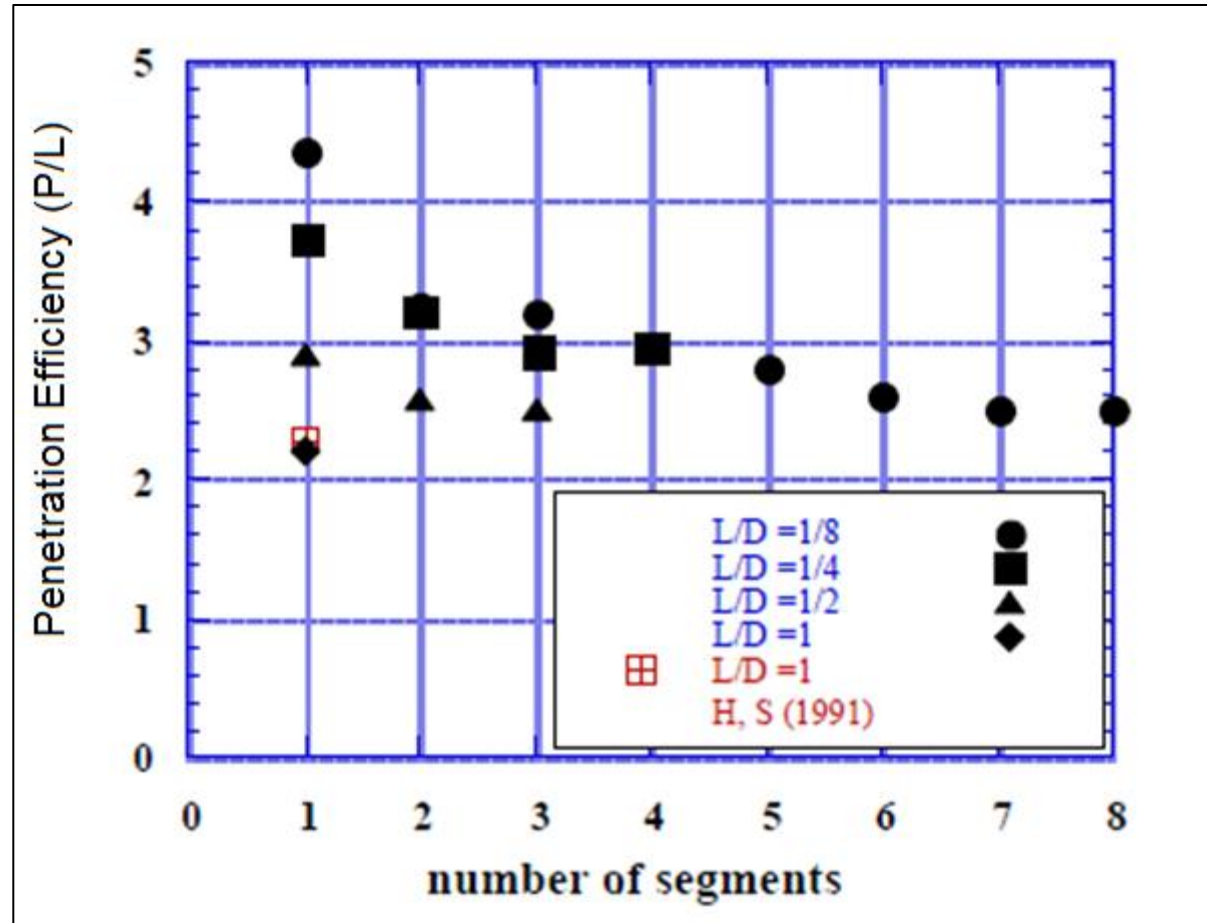
Figure 1.3. Penetration efficiency (P/L) versus number of segments for 4 different segment aspect ratios of tungsten heavy alloy impacting RHA (4340) steel at 2.6km/s. [7]
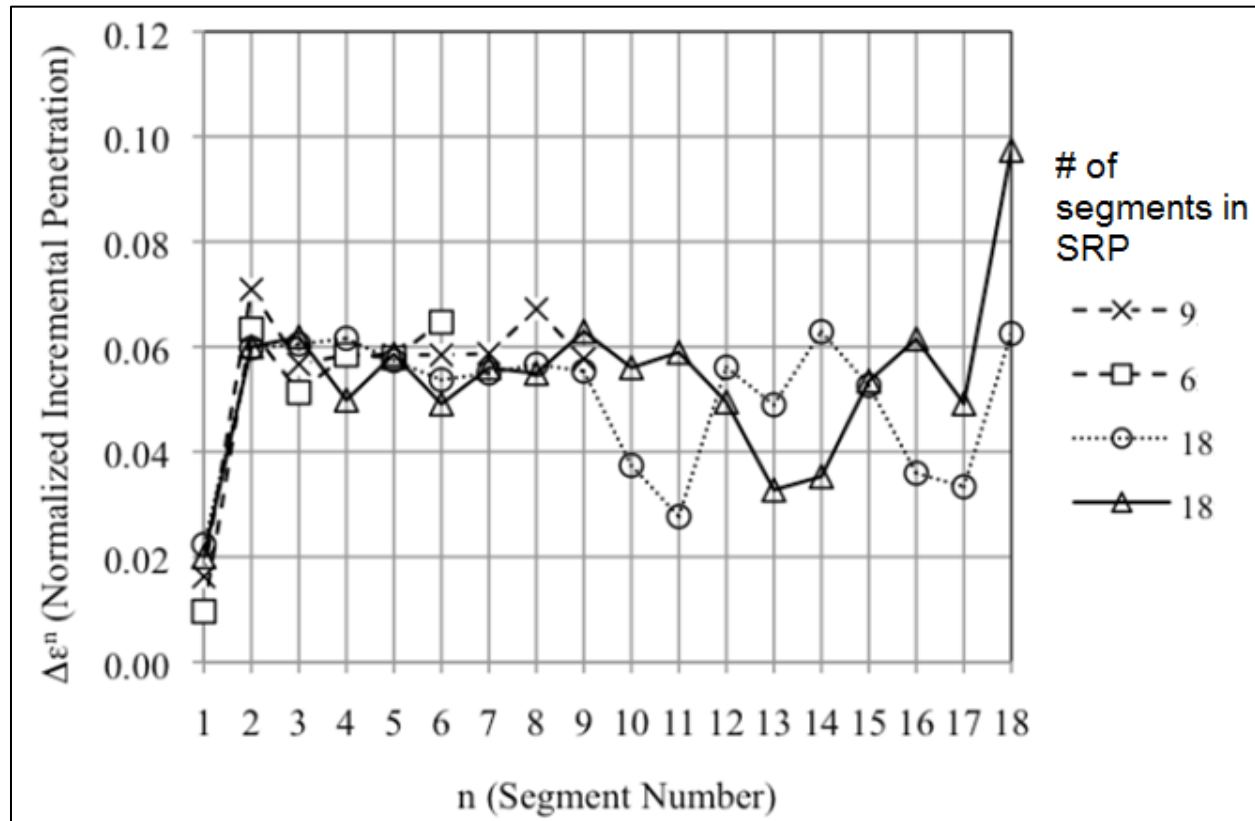
Figure 1.4. Experimental segment (91% W, 7% Ni, 3% Co tungsten alloy) penetration efficiencies impacting RHA (4340)

steel at 2.13km/s [30]

The enhanced performance of segmented penetrators must be taken in context: it is only useful if it can be harnessed. There are several factors demonstrated in literature which detract from a segmented penetrator's overall performance. Segmented penetrators are typically launched with spacers or with threaded connectors composed of light metals or plastics as shown earlier in Figure 1.2. In the case of spacers, there can be a considerable problem with yaw during segment flight. In the experiments of Hohler and Stilp, segments deviated from their trajectory by as much as 0.6 of their diameter [20]. If the launch package is too long, it will buckle upon launch and will have significantly reduced lethality.

There are difficulties which are not launch related. One such problem is cavity occlusion. Cavity occlusion is problematic as it hinders entry of subsequent projectiles and thus lowers penetration efficiency for segmented projectiles. Chou and Toland [32] studied the effect of occlusion by firing duplex rounds into pre-drilled holes in homogenous lead blocks. A duplex round consists of two projectiles: a leading projectile and a trailing projectile. The trailing projectile has a hole bored through the centerline which allows a portion of the propelling gas to pass through and propel the leading projectile while allowing the desired spacing. This spacing was varied to minimize the occlusion effect, which thereby determined optimal spacing between the projectiles. It was found that the maximum occlusion did not occur at an infinity of space between projectiles, but at some intermediate time. It should also be noted that while the Chou experiments were performed using a modified Sptizer-type of bullet, similar occlusive effects were observed in the experiments of de Rosset [33] which used a long rods of L/D ratio ranging from 9 to 1.5.

As most of the simulation results pertained to the subject of segmented rod penetration is kind of outdated, the present work revisited and also reexamined this impact configuration utilizing a state-of-the-art Lagrangian finite element code with special algorithms to handle excessive erosion and contacts between fragments. It is important to fully understand the nonlinear phenomena associated with the complex interactions between the impacting segments so that various design parameters could be optimized for determining a most penetration efficient segmented rod projectile configuration. Based on the open literature review, these interactions have not been actively studied by researchers working in the anti-armor design studies. In the present computational simulations of segmented rod penetration into a thick steel target, new design concepts to optimize projectile efficiency are also considered and reported in the present study.

Chapter 2

MATHEMATICAL BACKGROUND

2.1 Shock Wave Propagation

There are three distinct requirements needed to solve impact problems: 1) shock wave propagation, 2) equation of state, and 3) the material constitutive equations. The shock wave propagation involves the equation of motion, stress-strain relations, and strain-displacement relations. It is also important that the shock discontinuity is treated through appropriate jump conditions involving conservation of mass, momentum, and energy. This section briefly describes these conditions for the sake of completion.

The Rankine-Hugoniot jump conditions are essential to the understanding of shock wave propagation which is a singular phenomenon. The discontinuity across the shock front required to satisfy the so called Rakine-Hugoniot jump conditions are based on conservation of mass, momentum, and energy. The subscripts in the proceeding equations indicate the current state and the previous state by 1 and 0, respectively. U is the shock velocity, u is the particle velocity, v is volume, and e is specific internal energy. Foregoing their derivations, the equations for mass, momentum, and energy conservation are:

$$\frac{\rho_1}{\rho_0} = \frac{U - u_0}{U - u_1} \quad (22)$$

$$P_1 - P_0 = \rho_0(u_1 - u_0)(U - u_0) \quad (23)$$

$$e_1 - e_0 = \frac{1}{2}(P_1 + P_0)(v_0 - v_1) \quad (24)$$

While these jump conditions do not constitute an equation of state, they are used as such, accepting any error that may result. It has been discovered through rigorous experimentation that the shock velocity is related to the particle velocity by the equation:

$$U = C_0 + su \quad (25)$$

where C_0 is the bulk speed of sound, and s is an empirical constant unique to the material. In high velocity impact problems, the thermodynamic pressures generated by the impact often exceeds Hugoniot elastic limit. To determine the stress state at a material point, the pressure is determined from an equation of state. The EOS can be written as relationships between shock velocity and sound speed as shown in equation 25. When the impact velocities are very high, this linear relationship will not be adequate to describe the nonlinear response between pressure and volume. Equation 25 could be modified to include high order terms, such as a quadratic term. Most computational codes implement a variety of EOS equations that explicitly describe pressure – volume relationships containing higher order terms in volumetric strain or relative density. In the EPIC simulations, the following form of the Mie-Gruneisen EOS is employed for both tungsten and steel.

$$P = P_H \left(1 - \frac{1}{2}\Gamma\mu \right) + \Gamma\rho \, (I - I_0) \quad (26)$$

Where,

$$P_H = K_1 \mu + K_2 \mu^2 + K_3 \mu^3 \quad (27)$$

K_1, K_2, K_3 are empirical constants, I represents internal energy per uint mass, I_0 is that quantity at ambient pressure and density, Γ is Gruneisen parameter, P_H is the Hugoniot pressure at density ρ, and μ is the relative density. Library constants were used from the EPIC code. In all hydrocodes that solve shock wave propagation problems, the total stresses are calculated from the sum of deviatoric stresses and the pressure obtained from the EOS. Since the deviatoric stresses are determined from the strength models, it is appropriate to employ viscoplastic models that include the effects of strain hardening, strain rate hardening, and thermal softening on strength.

2.2 Material Strength Models

Given the dynamic nature of material response during an impact event, simple quasi-static plasticity theories must be discarded. There are several different material strength models, such as Zereilli-Armstrong [34], Johnson-Cook [35], and Bodner-Partom [36,37] available in open literature for describing strength variation with respect to plastic strain, strain rate, and temperature. The Johnson-Cook (J-C) model is widely used in impact problems involving ballistic penetration and crash worthiness studies. In addition, the J-C model parameters are fairly straight forward to determine and are available for a wide variety of materials. The J-C model is given by the following relationship:

$$\sigma = [C_1 + C_2 \cdot \varepsilon^n][1 + C_3 \cdot \ln(\dot{\varepsilon}^N)][1 - T^{*M}] \quad (28)$$

$$C_1 = Static\ yield\ stress$$

$$C_2 = Hardening\ coefficient$$

$$n = Hardening\ exponent$$

$$C_3 = Strain\ rate\ coefficient$$

$$\dot{\varepsilon}^N = \frac{\dot{\varepsilon}}{\dot{\epsilon}_0}\ ;\ \ \dot{\epsilon}_0 = 1.0s^{-1}$$

$$M = Softening\ exponent$$

In the present work, both the tungsten and steel are described by the Johnson-Cook model. The corresponding parameters used in the numerical simulations are given in Table 2.1.

Table 2.1. Johnson-Cook parameters used in EPIC simulations [6]

Material	C_1 (MPa)	C_2	N	C_3	M
Tungsten	960	1.33E+09	0.85	0.06875	1.15
RHA (Steel)	792.208	509.523E+06	0.26	0.014	1.03

Chapter 3

MODELING AND SIMULATIONS

Performing numerical simulations of dynamic events holds many advantages over experimental methods. For one, the cost of a single set of experimental data is many times that of an extremely robust PC or workstation. The next is the ability to observe trends and identify penetration mechanisms through a parametric study. Simulations facilitate greater creativity and efficiency by allowing for multiple impact configurations to be modeled in a relatively short amount of time. The ability to rapidly make changes to the simulation configuration allows for rapid understanding of results. A wider range of parameters influence the penetration efficiency and therefore it is important to optimize them for narrowing down the most feasible projectile-target configurations. In the present study, one of the main objectives is to understand the complex interactions between not only the segment and the target but also the interactions between the segments themselves. The secondary objective is to compare the DOP results from the current study with the results reported by Normandia and Lee [7] using the AUTODYN code.

There are several commercial- and government-supported finite element and finite difference based codes that specifically handle shock wave propagation and projectile

penetration into targets. These codes are often called as "hydrocodes." One of the 'hydrocodes'

most used by the penetration mechanics researchers in government laboratories is the Lagrangian

code: EPIC. In the present work to study segmented rod penetration into a thick steel target

plate, the 2006 version of the EPIC code was selected. EPIC simulations were run on an Xi

system with a 2.67GHz Intel Core i7 CPU and 2.99GB RAM. Additionally, some simulations

were run on the Sequoia Cluster of the University of Mississippi Supercomputer. This server

contains nodes which run Dual Intel Xeon Quadcore E5420 "Harpertown" processors. These

supercomputer runs were performed in serial.

One feature of EPIC which makes it particularly useful for high velocity impact is

utilization of an element conversion algorithm. Once an element experiences a set level of

equivalent strain (default is 0.40) it is converted to a particle which behaves in a fluid manner.

There is also an "erosion" option to simply remove these highly distorted elements from the

calculations since the time steps become extremely small preventing convergent solutions.

3.1 EPIC Code Simulation Design

In EPIC simulations, a two dimensional axisymmetric configuration was used since the

projectile-target configurations used in this study are cylindrical. Normandia and Lee [7] did not

provide all of the model parameters for the tungsten that was employed for the projectile in their

study. However, in the present study, the material parameters were taken from EPIC's materials

library. The target material considered was 4340 (RHA) steel. The semi-infinite target

dimensions were: 200 mm in diameter and 200 mm in thickness.

To study the effects of mesh resolution, one fine and one coarse mesh were used. For the baseline mesh, each composite element measured 1 mm x 1 mm. The number of nodes and elements were: 40,645 and 80,512. For the fine mesh, each composite element measured 0.5 mm x 0.5 mm and the number of nodes and elements were: 160601 and 322048. Each composite element was composed of four triangular elements with a total of five nodes. In both the baseline and fine mesh cases a uniform mesh was used in both the target and projectile. While the coarse (baseline) mesh had two layers of elements for the segment, the fine mesh contained 4 layers.

The present study considered the number of segments as a design parameter. In literature, the case of the single segment is almost universally addressed so as to establish an optimum segment performance. However, for the given segment aspect ratio (disk-like), there has been little work done for multiple segments. Historically, short rod-like segments have been the subject of experiment and simulation. It has been demonstrated that the smaller the segment aspect ratio, the greater the gains in penetration efficiency over an equivalent monolithic rod. This ability to create greater penetration with the same amount of projectile mass is the basis of the current work. Orphal et al [21] determined that the optimum aspect ratio for tungsten segments impacting 4340 steel was 1/8 for an impact velocity of 1.5 km/s and 1/16 for 3.0 km/s. It was decided to use eight segments of L/D=1/8 as it allowed for direct comparison with the one set of simulation data which exists [7] and produces near-optimal penetration which can be achieved by segmented penetrators.

The purpose of these simulations was to compare the performance of EPIC and AUTODYN by attempting to recreate the simulations of Normandia and Lee [7]. In their work,

the spacing parameter between each segment was eliminated by performing the calculations of successive segments one at a time into the recovered target after the individual segment penetration processes came to a complete stop (but before elastic rebound). However, in the present study, the spacing was explicitly considered. This spacing was achieved in the present work by a process of several steps, repeated for each segment. For reference, the currently impacting segment will be referred to as segment, n, and the impending segment will be segment, n+1. Initially the two segments were conservatively spaced far apart (8 cm). A tracer particle was placed on the front edge of segment n+1. When the DOP reached its maximum due to the penetration of segment, n, impacting, the position of the tracer particle and the crater depth were compared. This distance was then subtracted from the initial 8 cm spacing, thus giving the ideal segment spacing. This spacing estimation was continued for each of the segments. Figure 3.1 illustrates the initial configuration of the eight segment SRP in which the spacing between adjacent segments was not uniform.

In addition to the comparison of Normandia and Lee's work [7], simulation results were compared between the baseline and fine meshes. As the basis for SRP's is to produce more penetration than their equivalent monolithic rods, simulations were also conducted to verify this improvement. Before proceeding with such comparison study, the numerical artifact of certain assumptions used in the EPIC code, especially in handling highly distorted elements, is discussed in this section.

EPIC 2006 handles highly deformed elements using two different options, both of which are based on a critical value of volumetric strain in an element. The first option (conversion) converts the over-strained element into a particle which behaves as a fluid but retains the element's mass. The second option (erosion) removes the over-strained element from the
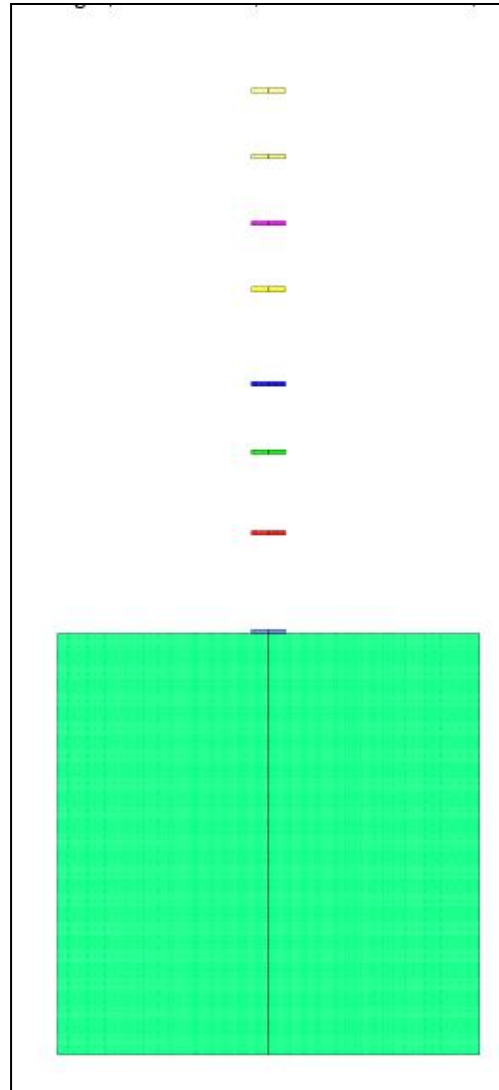
Figure 3.1. Initial configuration of 8-segment SRP with segment L/D ratio of 1/8 used in EPIC simulations

calculations. With erosion, the user decides whether to maintain the mass at the nodes or not.

Additionally, EPIC 2006 provides an option in which the projectile elements can be converted

entirely into particles before the simulation begins. When the erosion option that retains the

highly distorted element mass as a particle is used in the simulation, an anomalous particle

penetration along the centerline of the target (Figure 3.2) was observed. In this particular run,

only a two-segment SRP was considered since numerical instabilities prevented an investigation

of the full eight segments. Therefore, the erosion without element-to-particle conversion option

was not used in rest of the simulations presented in the following sections.

3.2 The Ejecta Phenomenon

The impact by the "flyer" plate like penetrator (first segment) generates a uniaxial strain

state during the first few microseconds after the impact. Compressive shock waves propagate in

both the target and first segment. The shock stress levels as per the pressure contours in Figure

3.3 reach well above the Hugoniot Elastic Limit (HEL) of both steel and tungsten. As per the

following shock relationship for planar impact:

$$\sigma_{shock} = \frac{Z_{tungsten} + Z_{Steel}}{Z_{tungsten} Z_{steel}} V_I \quad (29)$$

where Z is the impedance of respective materials. For the impact velocity of 2.6 km/s, the shock

stress is about 82 GPA; this is in agreement with the pressure levels as shown by the contour

plot. But due to the complex interactions between the reflected waves from the lateral surfaces

and the edges, the pressure contour plot shows different levels of pressure in both the segment

and target.
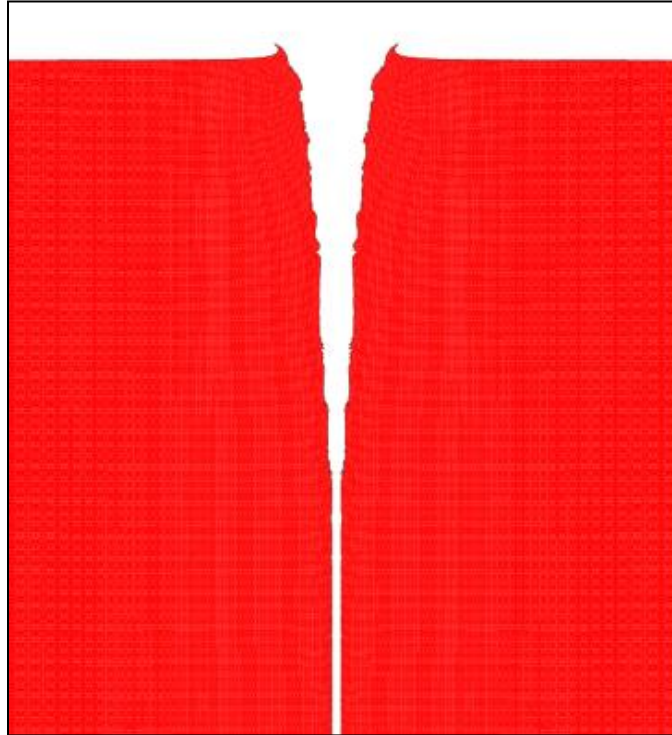
Figure 3.2. Final configuration of 8 segments using element erosion which retains nodal mass
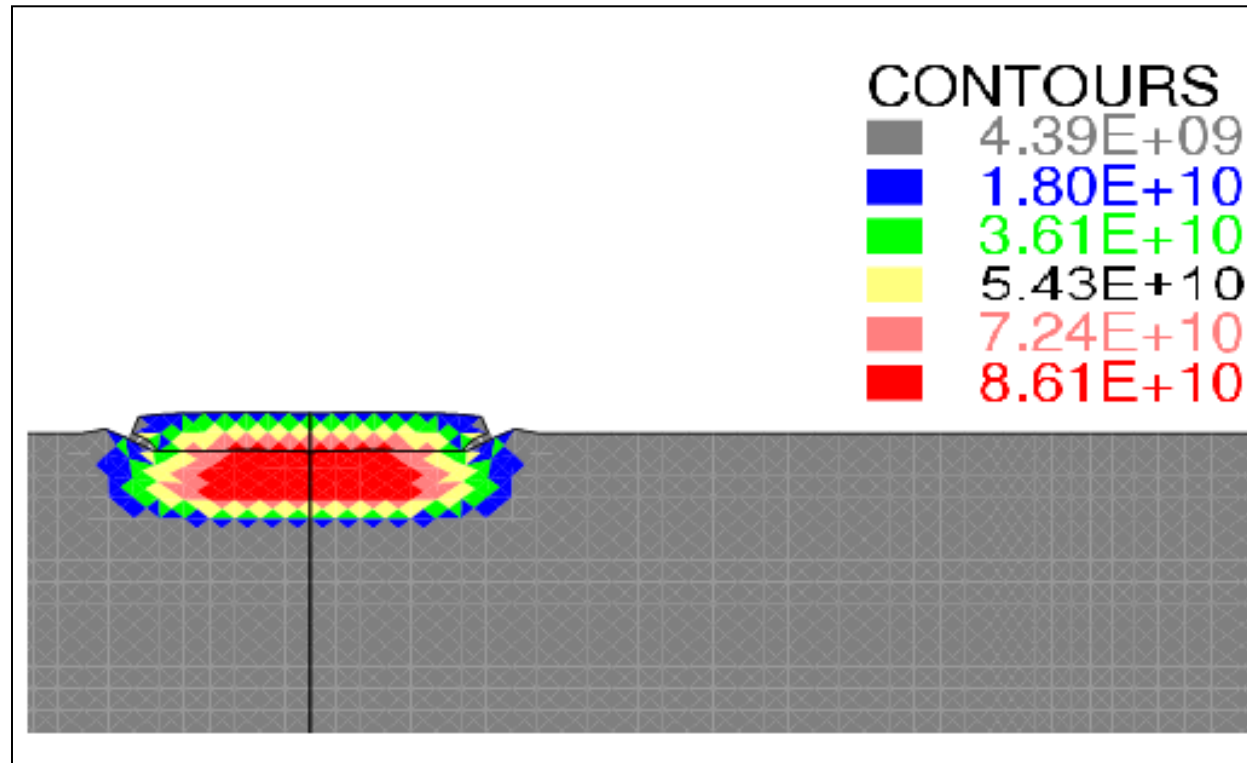
Figure 3.3. Pressure distribution (in Pa) at t=0.5µs for one-segment impact (fine mesh)

In the preceding section, a simulation setup of multiple collinear impacts of tungsten discs was discussed. The segmented rod penetrator concept is predicated on reconfiguring the mass of a long rod penetrator, the result of which is greater depth of penetration. One interesting facet of the segmented penetrator which will be discussed in further detail in the forthcoming sections is the phenomenon of backward flowing crater ejecta perforating incoming segments. The projectile-target configuration plot from the EPIC code using particle conversion algorithm is shown in Figure 3.4 for a 2-segment projectile penetration at an impact velocity of 2.6 km/s. After the initial penetration of the first segment into the target, ejecta consisting of both the target and first segment materials emanates from the penetration cavity and flowing backwards towards the incoming second segment. By 23 microseconds, the first segment has completely eroded away and the tungsten material is deposited entirely along the crater wall. It can be seen from Figure 3.4 ejecta was formed from the bottom of the crater towards the second segment. Before even this segment penetrated the steel target, some of its mass had been eroded away by the ejecta; however the penetration continued further until about 42-45 microseconds. The DOP at 23 microseconds was about 10 mm and the final DOP eventually was more than doubled (22 mm). It has been shown by Normandia and Lee [7] that once the ejecta is removed from calculations, the penetration efficiency of each segment remains nearly constant. Table 3.1 lists the depths of penetration with residual tungsten included and excluded in the Normandia and Lee [7] calculations.

The effects of ejecta on DOP were further studied through several EPIC simulations in which certain parameters were systematically varied. The parameters are: 1) erosion strain, 2) mesh size, 3) segment spacing, 4) segment shape, and 5) striker velocity. The following sections

31
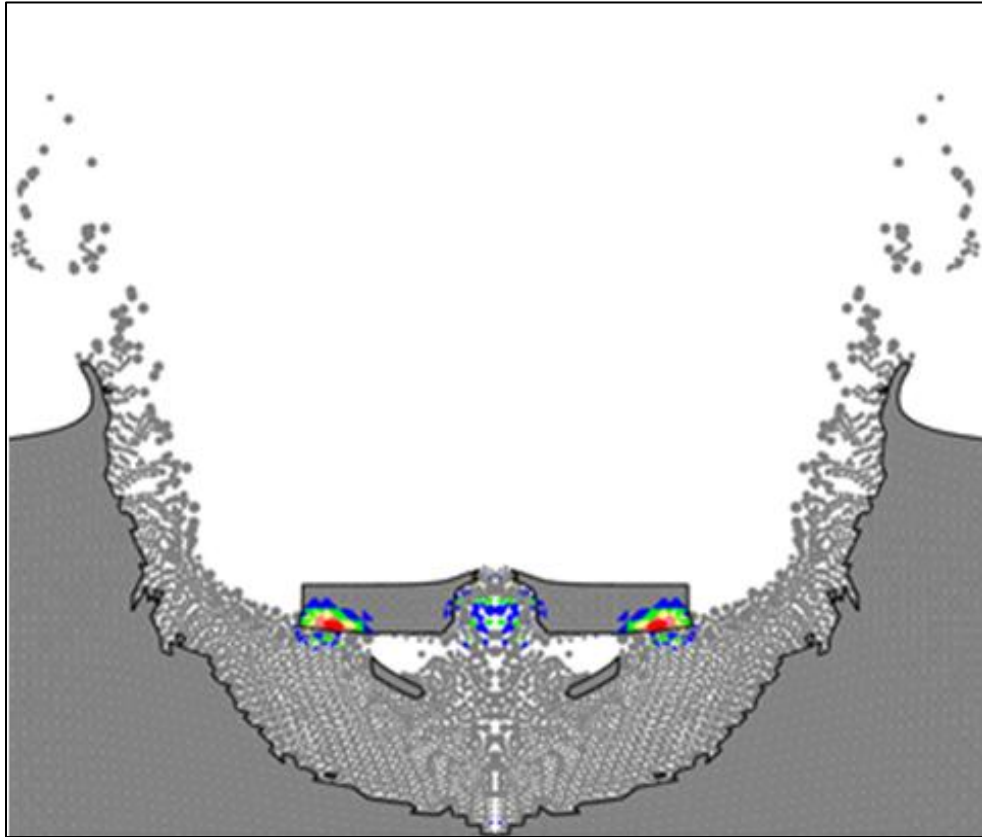
Figure 3.4. The penetration configuration at t=23µs for a 2-segment impact

Table 3.1. Penetration results for L/D=1/8 segments with and without residual tungsten [6]

Segment #	With Residue			Without Residue		
	P	P/L	P_{total}/L_{total}	P	P/L	P_{total}/L_{total}
First	8.7	4.35	4.35	8.7	4.35	4.35
Second	6.5	3.25	3.80	8.5	4.25	4.30
Third	6.4	3.20	3.43	8.6	4.30	4.30
Fourth	5.9	2.95	3.31	8.5	4.25	4.29

will present results from several EPIC code simulations to address various parameters on

projectile penetration depth into the target.

Chapter 4

RESULTS AND DISCUSSION

The penetration efficiency of a tungsten segmented rod projectile (SRP) is investigated through several EPIC simulations. The penetration efficiency is directly determined from the depth of penetration (DOP) into the thick steel target. The question is, for the same mass of SRP and striker velocity, how to obtain an optimum or deeper penetration by varying a) the space between the segments, b) the L/D ratio, and c) modifying the segment shape. Results from the EPIC code showed significant effects of erosion on DOP. To determine an appropriate element conversion algorithm for the SRP problem, a detailed exercise has been performed by repeating the simulation with different erosion options that were discussed earlier in Chapter 3. Since the final DOP and the time history of DOP as determined from the EPIC code are employed in the comparison study between various projectile configurations and striker velocities, it is necessary to discuss how these information or data are extracted from the simulations. Therefore, it is indeed important to establish how the DOP is estimated or determined from the EPIC code.

4.1 Erosion and DOP

The DOP was assessed using an intrinsic function in EPIC which tracked the minimum z-coordinate of the projectile as a whole. Due to complex interactions (or motions) between the projectile (tungsten) and target (steel) mass particles in the cavity vicinity, slight inaccuracies could occur in the estimation of DOP, especially during the final phases of the penetration process. Figure 4.1(a) shows an example of a configuration where the minimum z-coordinate function accurately predicts the depth of penetration. Figure 4.1(b), on the other hand, illustrates material mixing which produces a degree of artificial penetration. Unfortunately, such numerical artifacts make determination of DOP less ambiguous and generate sometime anomalous data. The work of Normandia and Lee [7] is compared in Table 4.1 with the current work. They also examined the effects of residual penetrator matter on the depth of penetration. Their DOP simulations with and without residual crater matter was presented earlier in Chapter 3 through Table 3.1.

Overall, EPIC's Lagrangian results showed very good agreement with Normandia and Lee's [7] AUTODYN results. Normandia and Lee's data [7] shows a clear leveling in penetration per segment. The penetration produced by the EPIC 2006 simulations possess a similar trend but with a few anomalies. Penetration for the second and sixth segments was abnormally high. These disparities can easily be attributed to the method of DOP determination as material mixing was shown in Figure 4.1(b) to produce an artificially deep projectile minimum z-coordinate. Additionally, it is possible that the complex mechanics of the interacting meshless particles caused unforeseen irregularities in penetration.

Table 4.1. Penetration comparison between AUTODYN and EPIC 2006

Segment #	AUTODYN Penetration Depth (mm)	EPIC 2006 Penetration Depth (mm)
1	8.7	10.0
2	6.5	11.2
3	6.4	6.2
4	5.9	6.3
5	5.6	3.6
6	5.2	7.3
7	5.0	5.1
8	5.0	2.0
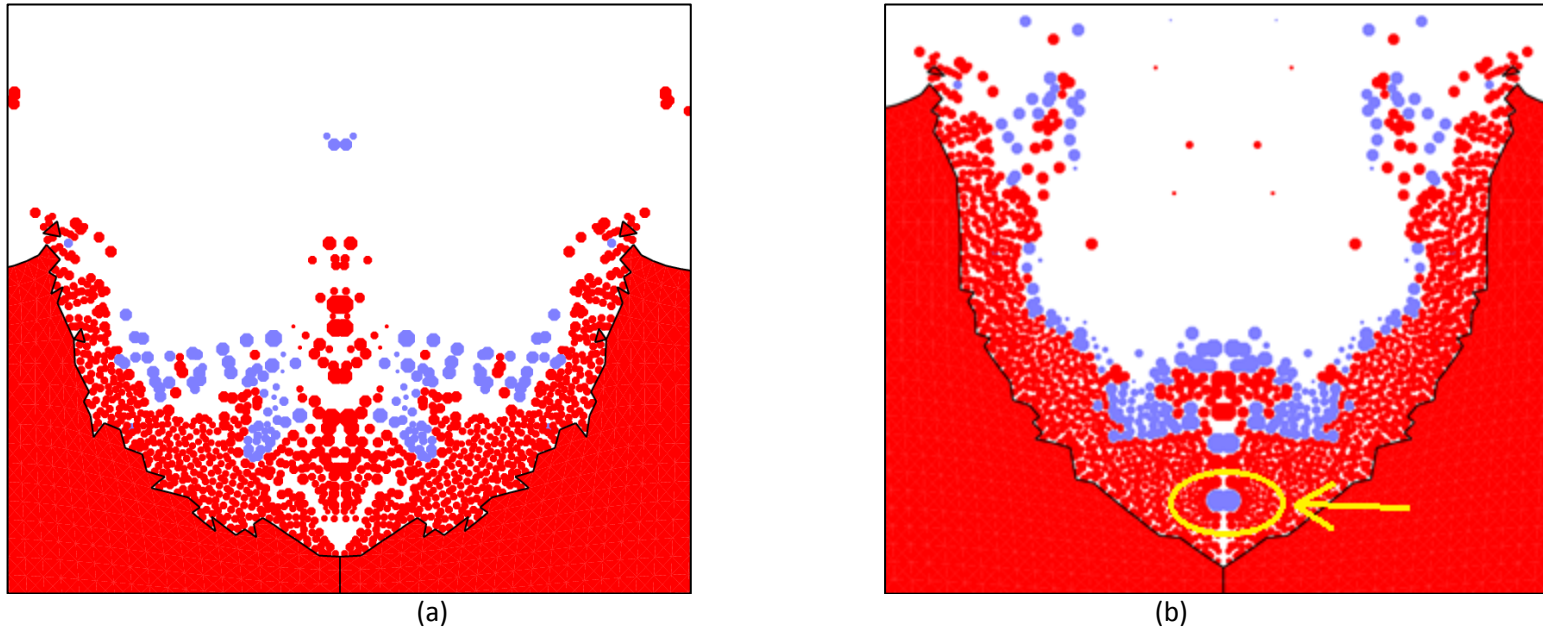
Figure 4.1. (a) Final configuration where minimum z-coordinate function accurately measure bottom of the crater for a projectile impacting at a velocity of 2.6km/s; (b) Example of possible inaccuracy in minimum z-coordinate estimation due to material mixing during 2nd segment impact at the bottom of the crater as indicated by the arrow.

To further validate, the crater morphology as observed in an experiment in which a long rod tungsten projectile penetrated a thick steel target was compared with the EPIC generated crater. A noticeable aspect of the crater morphology found while using SRP is that of scalloping. Examples of scalloping are given from previous works in both the computational (Figure 4.2) and experimental (Figure 4.3) realms.

The normalized crater diameters due to the impact of first segment determined by AUTODYN (seer Normandia and Lee [7]) and present EPIC simulation were also compared. The crater diameter from AUTODYN was 1.61 while for the EPIC results utilizing element conversion was 1.68 which is a difference of only 4%. At the other extreme, the normalized crater diameter of the impact configuration utilizing Type 1 erosion (removed distorted elements while retaining nodal mass) differed from Normandia and Lee [7] by 45%. They also presented a schematic of typical deep crater observed in experiments as shown in Figure 4.2.   According to Tolman et al.[30], the scalloped crater edges are characteristic of segmented rod impact as shown in Figure 4.3.

Scalloping is difficult to observe when utilizing EPIC's particle conversion algorithm. However, it is much more pronounced when using the two different erosion algorithms (Figures 4.4 and 4.5). Another feature of crater morphology explored was the crater diameter. Table 4.2 lists the crater diameters for particle conversion, erosion type 1, and erosion type 2 algorithms. These results were compared with the diameter obtained by Normandia and Lee [7]. However, the EPIC results in Figure 4.4 for a two segment impact configuration using type 1 erosion exhibited somewhat over-exaggerated slope of the crater and an unrealistic crater shape as
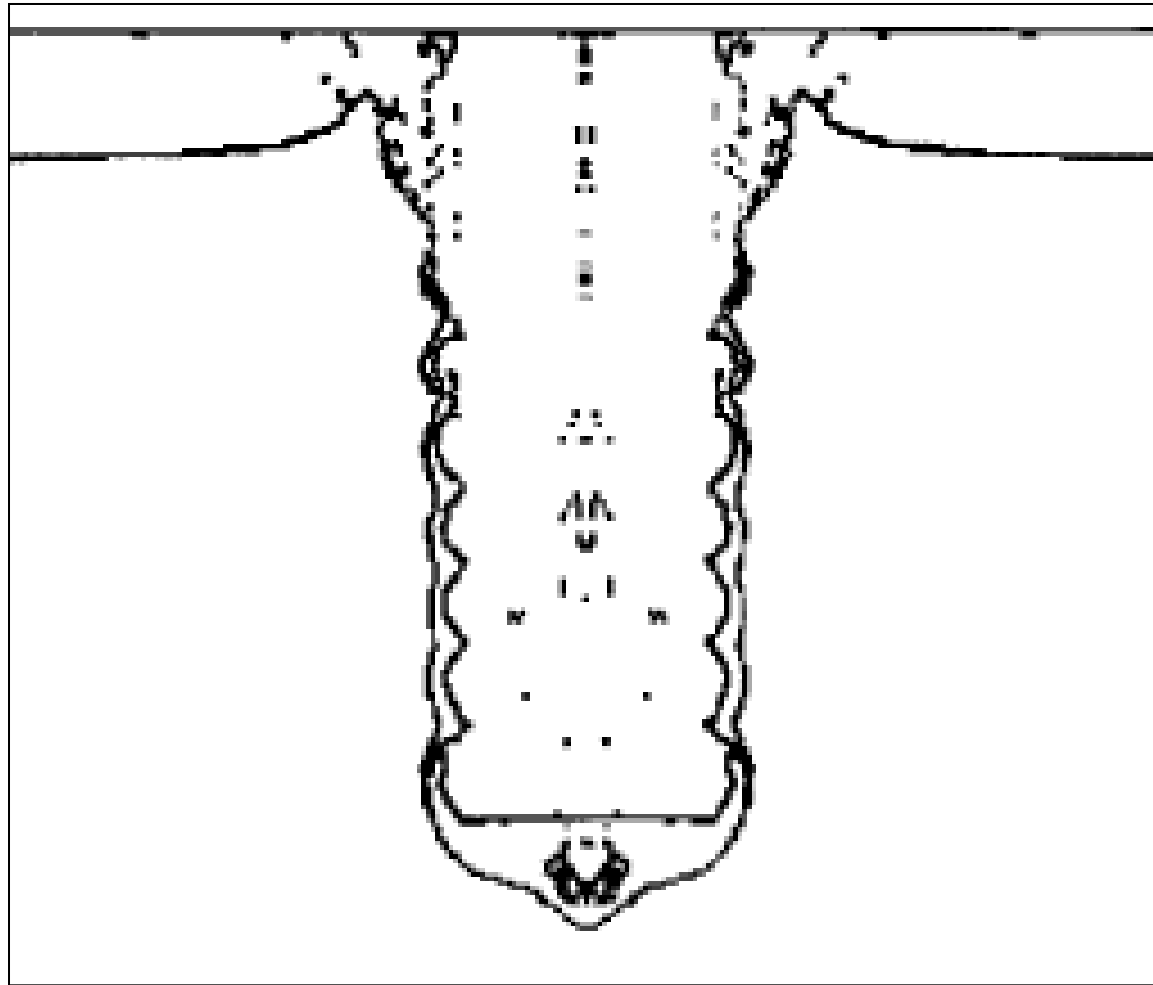
Figure 4.2. Example of crater scalloping in simulation [7]
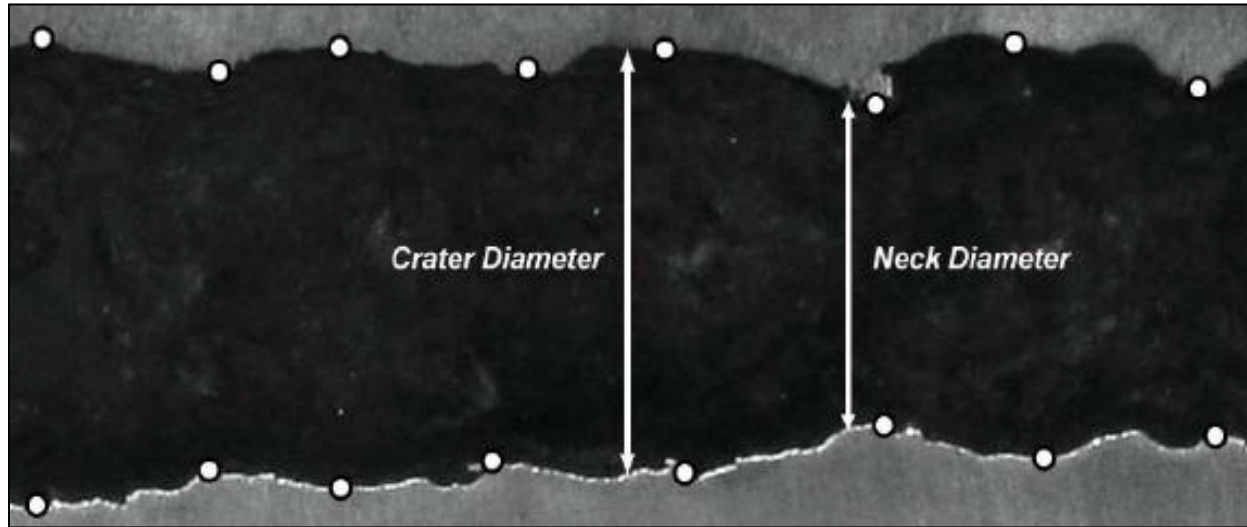
Figure 4.3. Example of crater scalloping in experiment [30]
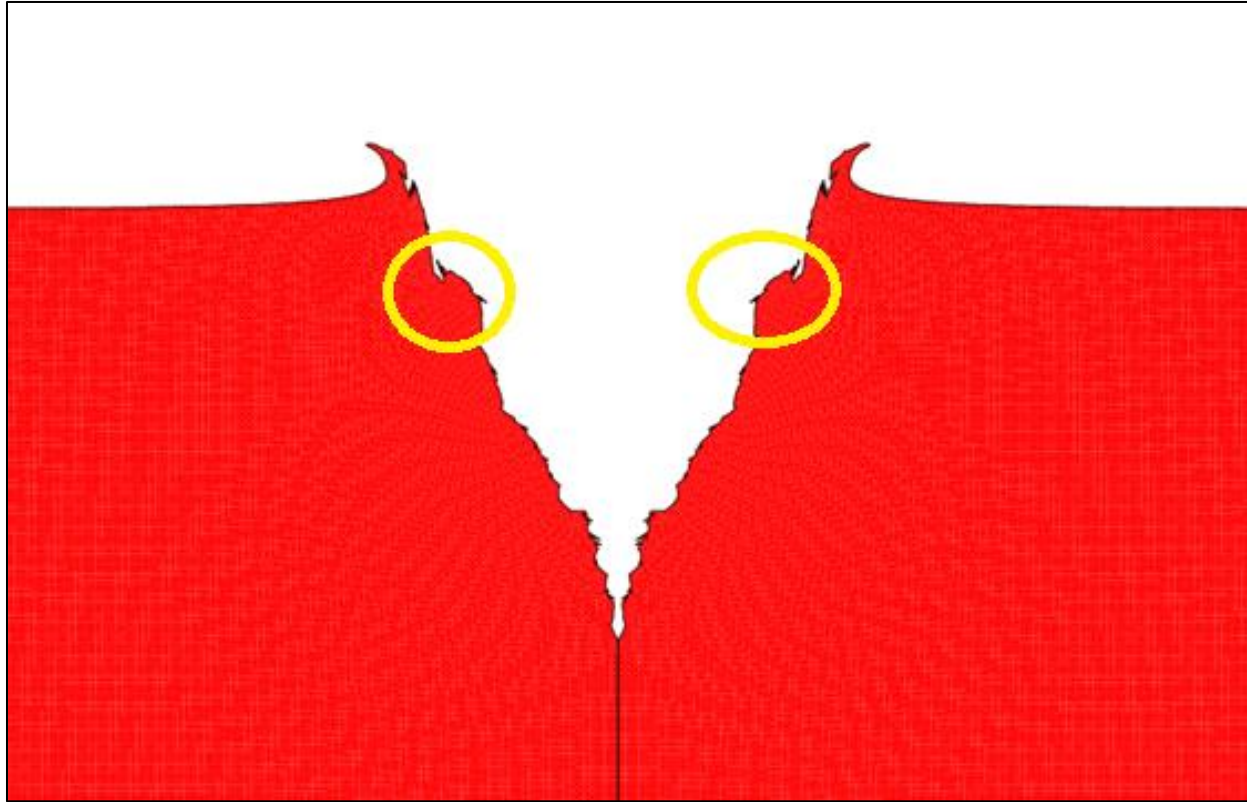
Figure 4.4. Final configuration of two segment impact at 2.6 km/s using type 1 erosion algorithm with crater scalloping highlighted
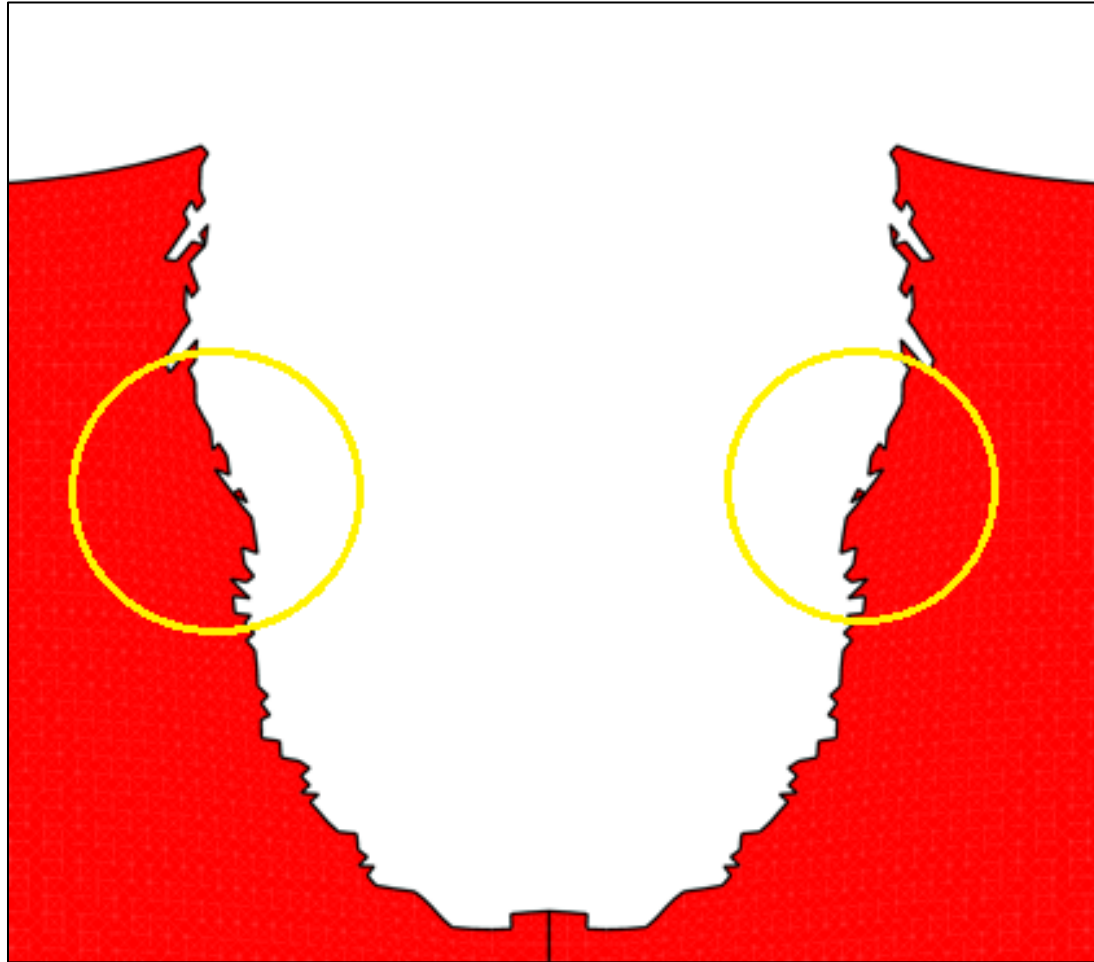
(fine mesh)

Figure 4.5. Final configuration of two segment impact at 2.6 km/s using type 2 erosion algorithm with crater scalloping highlighted

(fine mesh)

Table 4.2. Crater diameters normalized by segment diameter

Simulation Type	D_1/D_{seg}	D_2/D_{seg}
Conversion algorithm	1.68	1.01
Type 1 erosion algorithm	2.33	1.27
Type 2 erosion algorithm	1.25	1.04
Normandia and Lee [6]	1.61	N/A

compared to experiments (see Figure 4.3). The scalloped edges of the crater observed in type 2 erosion (Figure 4.5) are far closer to the demonstrated examples of proper crater scalloping.

For all types of simulations, the second normalized crater diameter was smaller than the first which indicates crater necking (see Figure 4.3) which agrees with Tolman's work [30]. Table 4.1 compares the normalized diameters of the crater formed by the first and second segments for various erosion options in the EPIC code. It appears that type 2 erosion seems to compare well with element-to-particle conversion algorithm, especially the smaller crater diameter. This validation provides additional confidence in using a suitable and realistic erosion option for determining depth of penetrations from EPIC simulations.

4.2 DOP comparison of Single Long Rod versus SRP

To further validate the concept of increased penetration by a segmented rod, the depth of penetration comparison between the 8-segment SRP and its monolithic equivalent is provided in Figure 4.6. By 50 microseconds, the penetration process is ceased in the single long rod case while the SRP took about 150 microseconds to complete the penetration process. The DOP in SRP was 25% more than the DOP by the single solid rod. These simulations further validated that increased DOP could be obtained using SRP. The stair stepping of the DOP as time progressed can be seen from Figure 4.6. As each segment completed its penetration and while the cavity bottom elastically rebound, the subsequent segment arrived to begin its penetration into the steel target. In this simulation, an optimum spacing estimated from several trial EPIC runs was used so that maximum DOP could be achieved following the discussions by Normandia and Lee [7]. The monolith reaches its maximum penetration depth much quicker than the SRP.
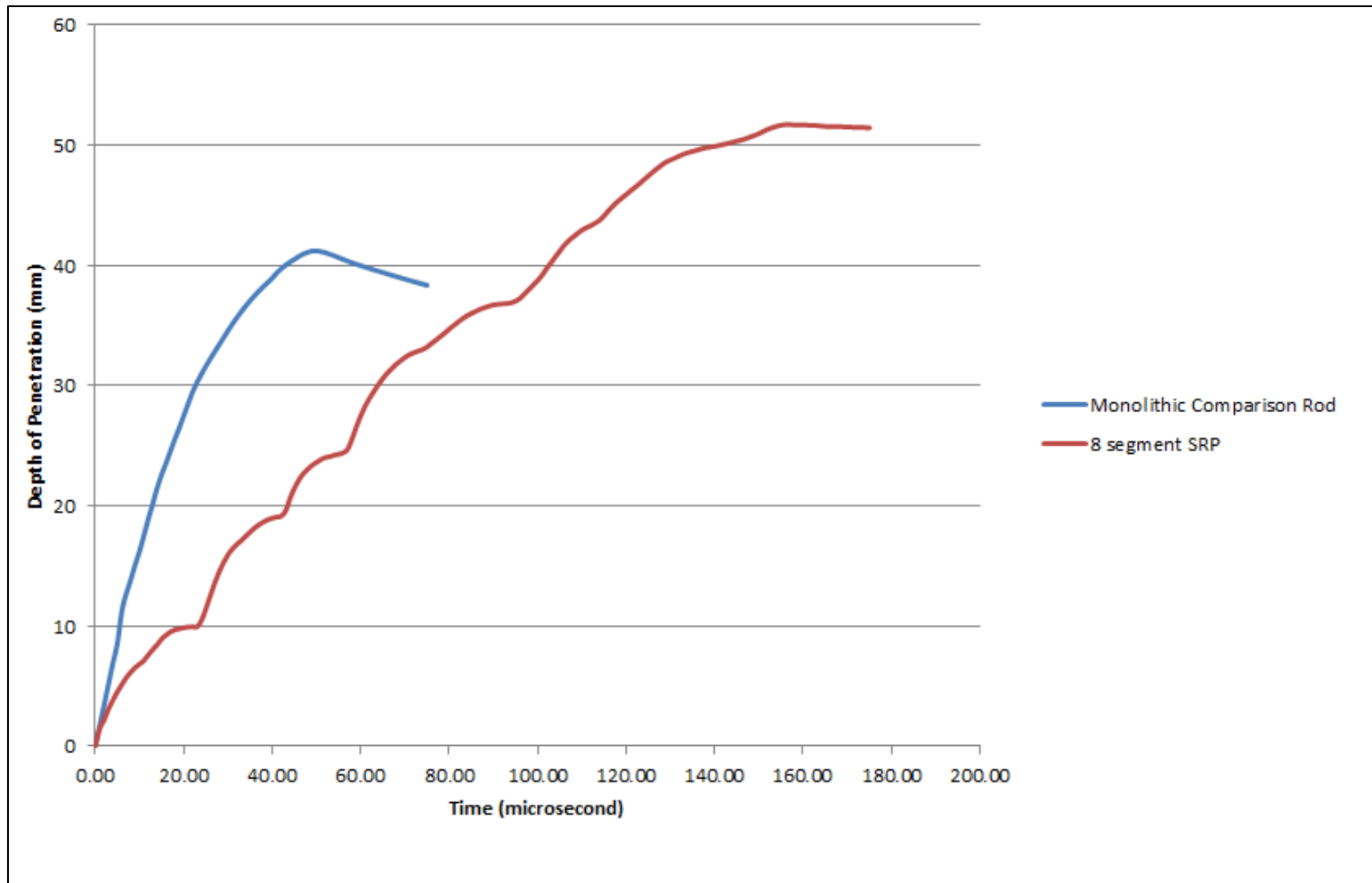
Figure 4.6. Depth of penetration comparison between 8-segment SRP and monolithic equivalent rod

95% of its maximum penetration was achieved in 39 µs whereas it took the 8-segment SRP 141 µs to achieve this same percentage. The average rate of penetration to 95% of its max is 1.07 mm/µs for the monolith and 0.42 mm/µs for the 8-segment SRP.

Since 8-segment rod simulation is computationally more complex as compared to a single solid rod case due to the interactions between various segments, it was necessary to compare the effect of mesh resolution on DOP. Figure 4.7 compares the time history of DOP for two different mesh resolutions that were described earlier in Chapter 3. The fine mesh showed about 4 -5% increase in final DOP as compared to the coarse mesh. The coarse and fine mesh predicted similar DOP history up to the impact by the 3rd segment and then started deviating slightly. For the first 50 microseconds, the average difference of DOP between the two mesh resolutions was 0.16 mm. From 50 to 125 microseconds, this average jumped to 2.09 mm. For the entire penetration process, the average was 1.12 mm. In general, the penetration process of the fine mesh closely mirrors the baseline mesh. Another important aspect for discussions is how the mass of each segment eroded away as the penetration process continued. The complexity of the erosion as well as the contact algorithm greatly influences the history of the erosion rate for each segment is shown in Figure 4.8. No sequence-of-time event could be consistently observed between the erosion rates of various segments. For instance, segment 3 (green) erodes slowly for about 12 microseconds prior to complete erosion. The ejecta phenomenon unfortunately throws several unforeseen complications in interpreting the numerical results from the EPIC code. The mass particles that were generated, based on the conversion algorithm, penetrate the incoming "subsequent" segments. As they eroded a significant percentage of mass in a premature manner; the overall penetration efficiency of the SRP is certainly degraded.
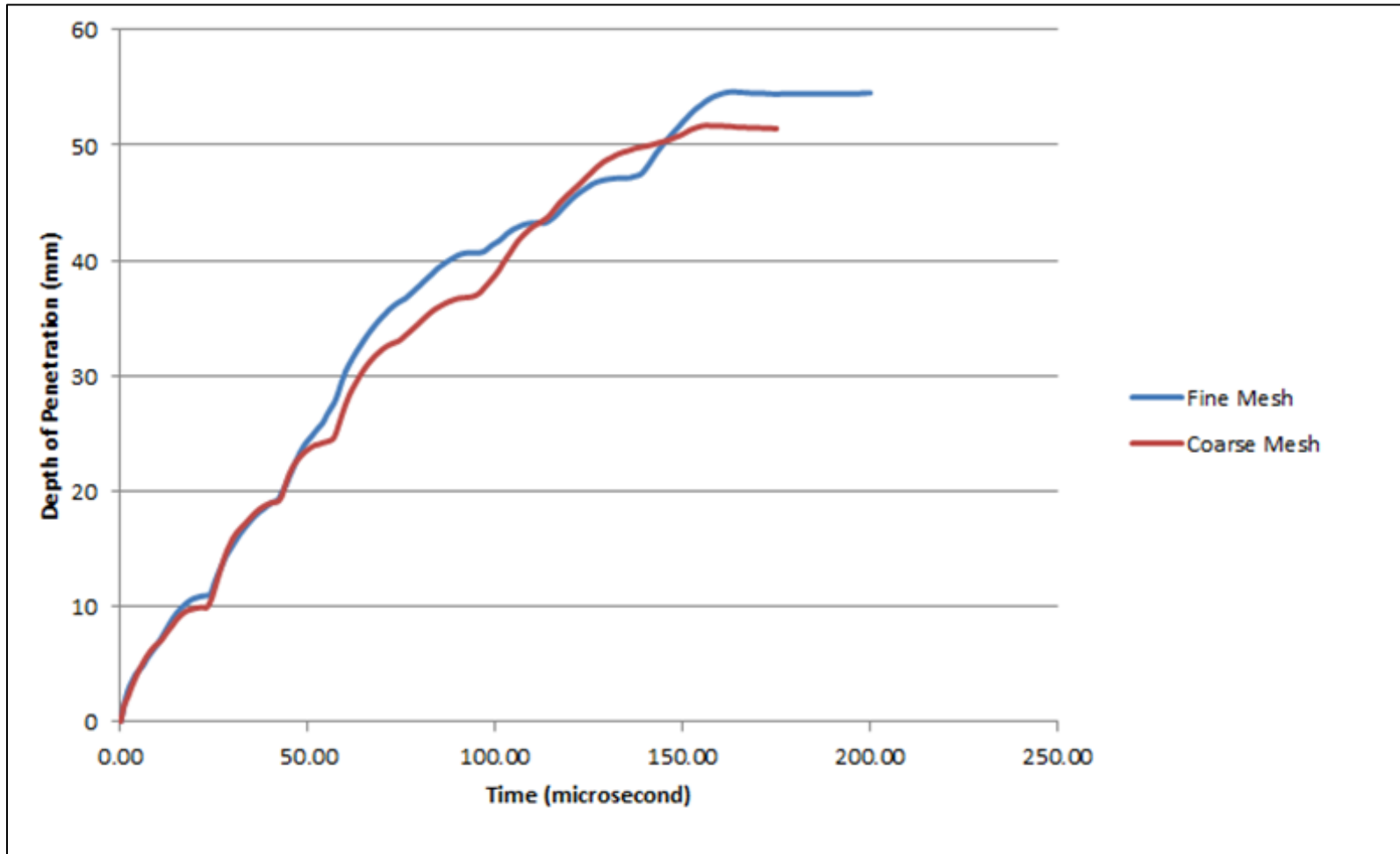
Figure 4.7. Depth of penetration comparison for 8-segment SRP with different resolution meshes
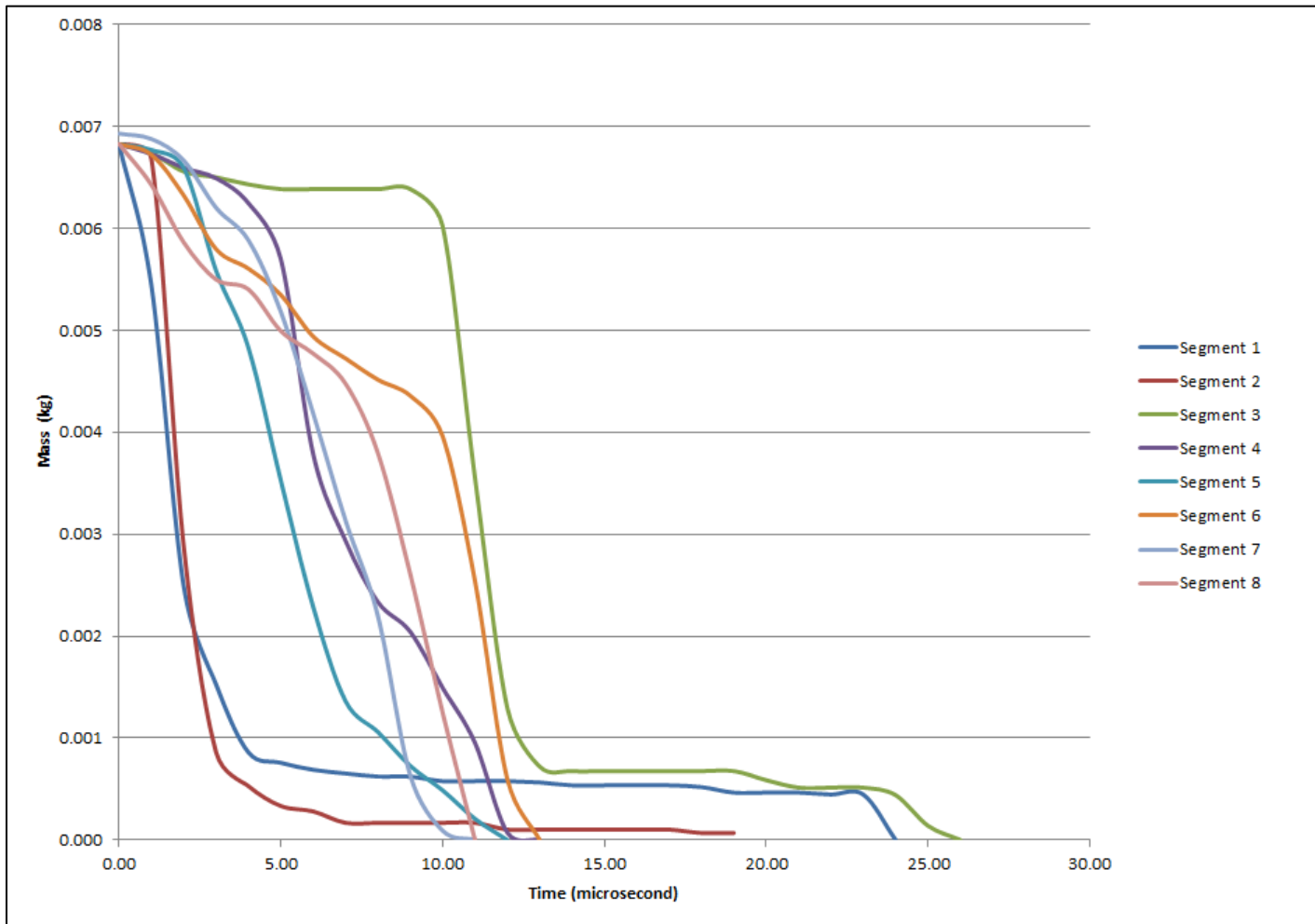
Figure 4.8. Mass versus time for individual segments

As was previously stated, incoming segments have significant interactions with backward flowing ejecta. Figure 4.8 quantifies the mass loss experienced by the segments as a function of time while Table 4.3 tabulates the time required for complete dissolution of each segment. Both Figure 4.8 and Table 4.3 pertain to an 8-segment SRP. The zero time for each segment in Figure 4.8 corresponds to the time when each segment starts to lose mass. Aside from the first segment, this zero time indicates the segments' first interaction with back flowing ejecta. The computational simulation of the interactions between the ejecta and the in-coming segment is extremely complex and highly nonlinear due to excessive deformation, element-to-particle conversion, and slide line algorithms. It is clear that there is no clear correlation between each segment's time taken to completely erode away. Table 4.4 presents a parameter, Δ, which measures the distance between the z-position at which the segment was fully converted into particles and the bottom of the crater. As more and more tungsten segments pile up at the bottom of the crater, the incoming segments due to the back flowing ejecta get eroded well before they start penetrating the target further. However, the pressure generated by the sequential impacts continues the penetration process and the DOP continually increases until after all segments impacted the crater surface.

For simplicity, the depth of penetration for various high-strain element conversion algorithms and impact velocities are shown only for a 2-segment SRP. For completion, the DOP results for the LRP are also presented at three different velocities: 1500 m/s, 2000 m/s, and 2600 m/s. As the impact velocity increased the amount of increased DOP between the SLR and SRP significantly increased as can be seen from Figure 4.9. The penetration ceases by 20

Table 4.3. Time for complete segment dissolution into particles

Segment Number	Time to Complete Dissolution of Segment (μs)
1	24
2	19
3	25
4	13
5	12
6	13
7	11
8	11

Table 4.4. Distance from crater bottom at which segment is completely converted to meshless particles (Δ)

Segment Number	Z-Position of Segment When Completely Converted to Particles (mm)	Minimum Z-Coordinate of Projectile (mm)	Δ (mm)
1	-9.7	-10.9	1.2
2	-17.2	-19.1	1.9
3	-22.9	-27.1	4.2
4	-22.7	-28.5	5.8
5	-29.1	-37.0	7.9
6	-28.3	-40.7	12.4
7	-33.9	-43.3	9.4
8	-32.4	-47.2	14.8
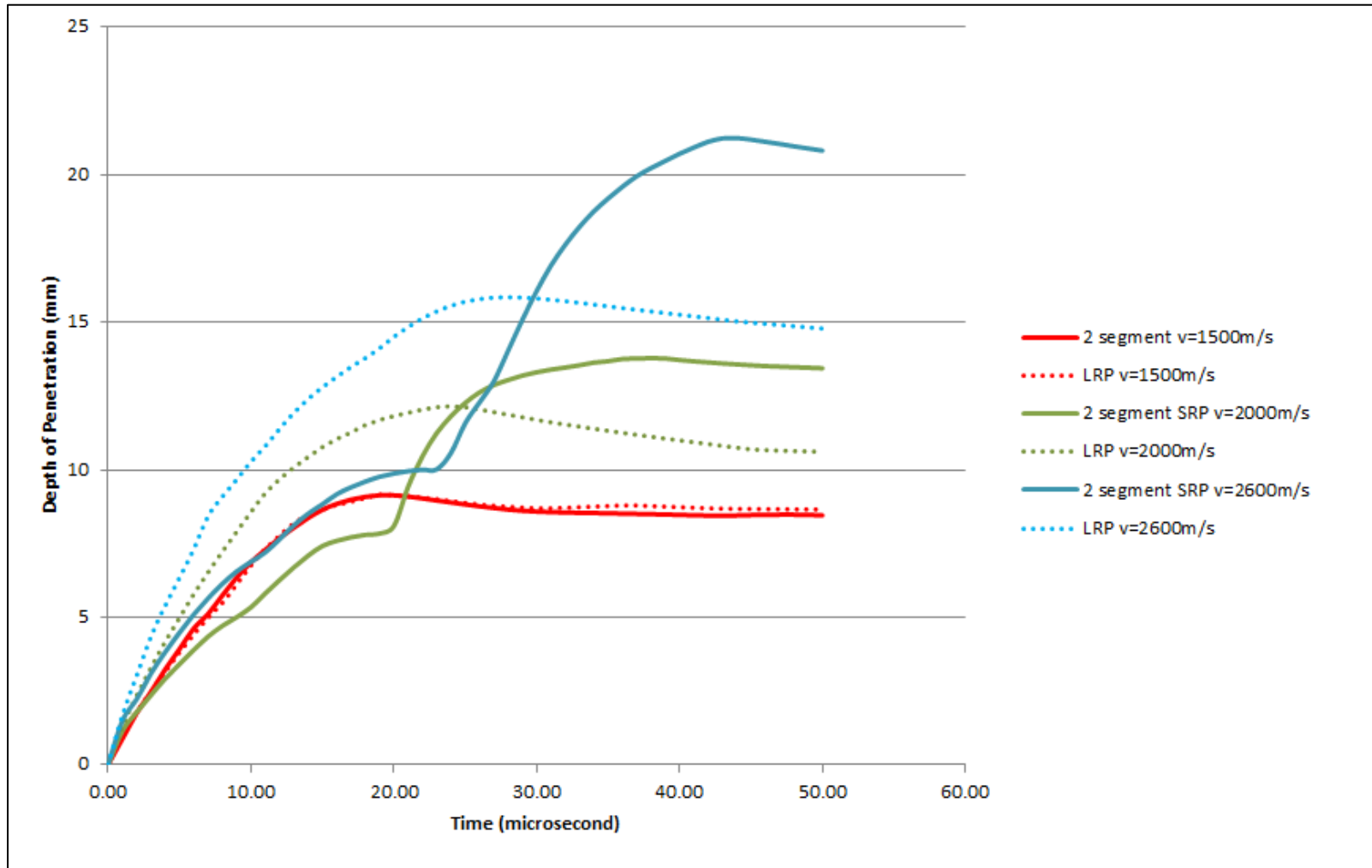
Figure 4.9. Depth of penetration comparison for 2-segment SRP with different impact velocities

μs for the lowest velocity (1500 m/s) in both cases and that is why there is no difference between the DOP time history.

An unexpected finding was that the crater ejecta flowed upward and perforating the incoming segment prior to that segment impacting the bottom of the crater. The crater "bottom" is defined as the top of the majority of the mass of the residual crater materials. It should be noted that the phrase "bottom of the crater" is somewhat tenuous as the many dispersed meshless particles within the crater make it difficult or even impossible to pinpoint exact bottom. The time for complete segment dissolution into particles due to this type of interaction with ejecta is tracked in Table 4.3. Segments 1-3 took an average of 22.7μs to be completely converted into particles while segments 4-8 took an average of 12μs. These latter segments were completely converted at a much greater height (designated as Δ in Table 4.4) above the crater bottom.

4.3 An Alternative SRP Design

Though it has been shown through various EPIC simulations that the ejecta indeed reduced the amount of kinetic energy of the subsequent segments due to premature erosion of segment mass, the overall penetration depth by a SRP is certainly higher than the DOP of a single long rod projectile. The natural follow-up question to this: is there a way to reconfigure the penetrator mass again to accommodate the ejecta? Since the majority of the ejecta has been shown to act along the axis of symmetry, a logical method of accommodation is to provide a path

54

for the ejecta to flow unimpeded along the axis of symmetry, thereby retaining the kinetic energy

and momentum of the segment. A simple method of accommodating the ejecta is to create a

hole in the segment (or disk) with the removed mass evenly redistributed on top of the resulting

washer-shaped projectile. The new SRP design will have the first segment as a solid disc and the

second segment as a washer (a disc with a hole in the middle). In EPIC simulations, five

different hole diameters for the second washer-shaped segment was considered: 2mm, 4mm,

6mm, 8mm, and 10mm as shown in figure 4.10.

The main objective of EPIC simulations of this alternative design is to test whether there

will be any gain in DOP over the standard SRP where all segments are solid discs. Using a fine

mesh, DOP versus time data was generated from the various EPIC simulations. Figure 4.11

shows a comparison between the DOP history for a standard 2-solid segment projectile and the

washer-disc based new design configurations for various washer diameters.   As the washer

diameter becomes larger, the DOP decreased showing reduction in the penetration efficiency of

the new design. The DOP difference, denoted by the variable delta, represents the percent

difference between the depth of penetration of a standard two-disc SRP and an SRP consisting of

one disc and one washer-type segment.

The depth of penetration for this design was compared with a two-segment SRP

consisting only of solid discs without a hole in the center. Four out of the five hole diameters

produced gains in penetration, though the gains were not significant compared to the solid discs.

The EPIC results showed a clear trend in DOP with respect to the hole diameter. As the

diameter increased, the final DOP tended to decrease with the exception of the 8mm diameter
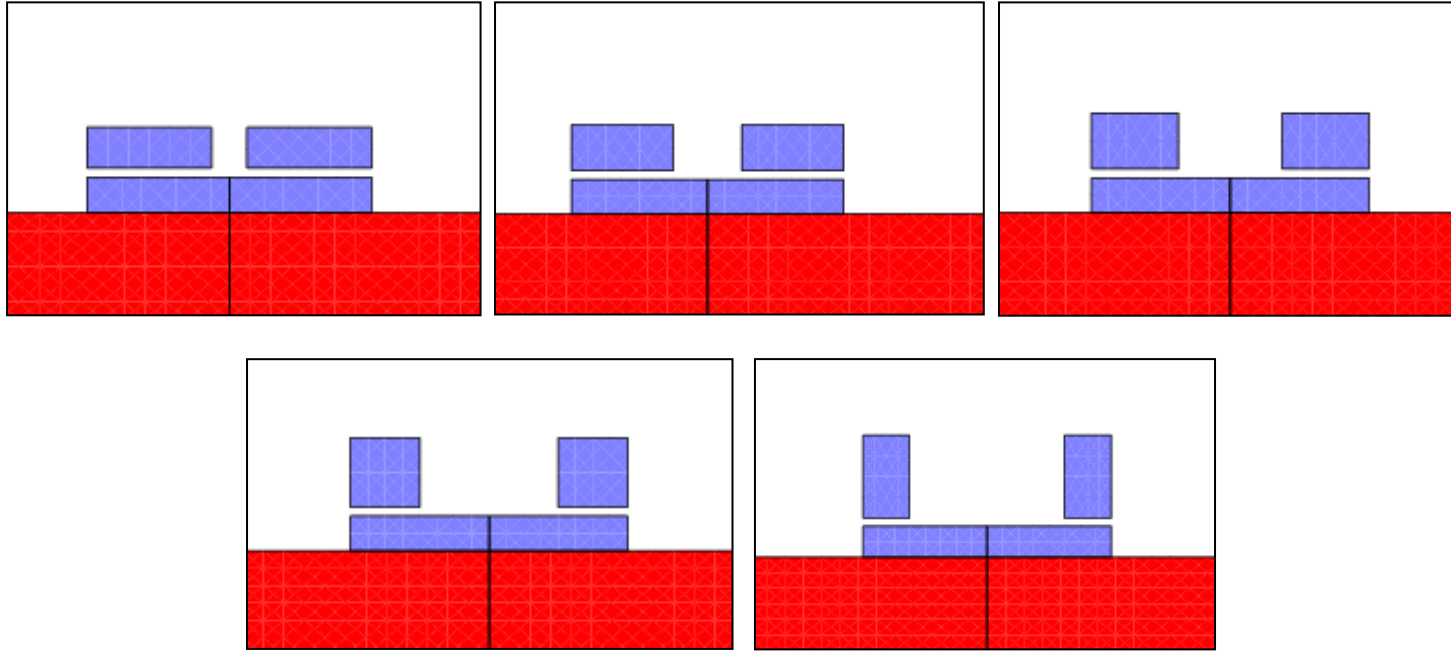
Figure 4.10. Initial configuration for five different inner diameter (top left to bottom right): 2mm, 4mm, 6mm, 8mm, and 10mm
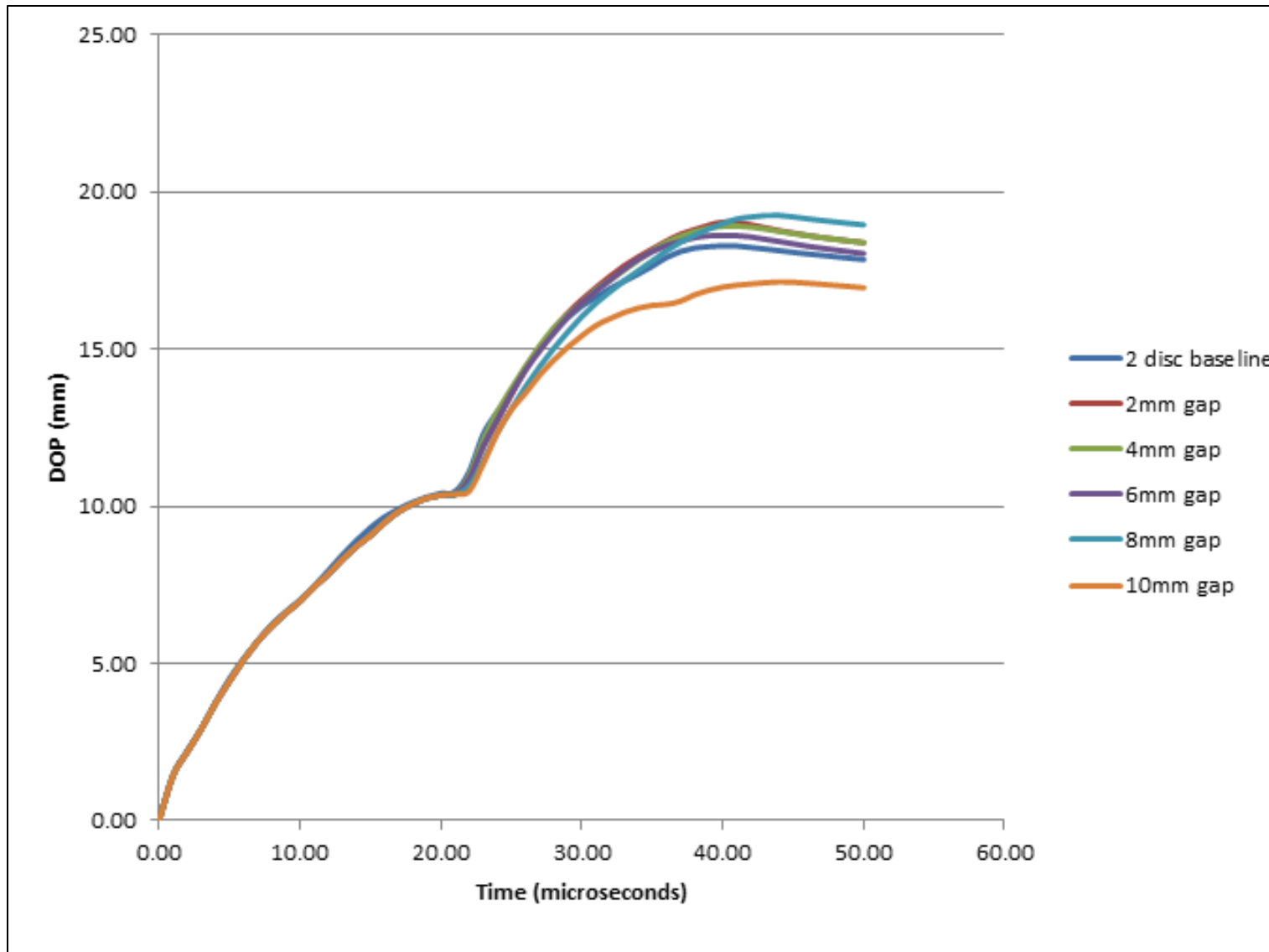
Figure 4.11. Depth of penetration of various hole diameters compared with two-disc SRP

hole. The configurations with 2 and 4 mm diameter hole exhibited identical time history of the

DOP.

To further examine the penetration capability of the new design, an EPIC simulation with

a 8mm hole diameter 8-segment SRP configuration was considered. The alternative SRP design

produced gains in DOP up to the end of the third segment's penetration process. However,

subsequent segment impacts confirmed that there was no advantage with the washer type discs to

gain more penetration into the thick steel target plate. For this new SRP design, any short term

gains made by initially accommodating backward flowing ejecta is offset in the later stages of

penetration by a decentralized ejecta plume.   Figure 4.12 demonstrates an example of the lack of

a coherent central jet during the later stages of segment impacts.   Another factor affecting the

efficacy of the alternative SRP design was the stress state induced by the segment geometry. A

thin disc (or plate) is an ideal geometry for inducing very high stresses due to a uniaxial strain

condition being imposed. The loading conditions move further away from this ideal. Once the

geometry is modified (as it was in the alternative SRP design), a final DOP of 40.42 mm was

observed, compared with 54.63 mm in the all-disc design. The final DOP dropped by 25% for

the new design; therefore it was very clear that a washer type design after all was not effective to

reduce the detrimental effect of ejecta. A time history of the DOP comparing the alternate

design with the standard design is featured in Figure 4.13.
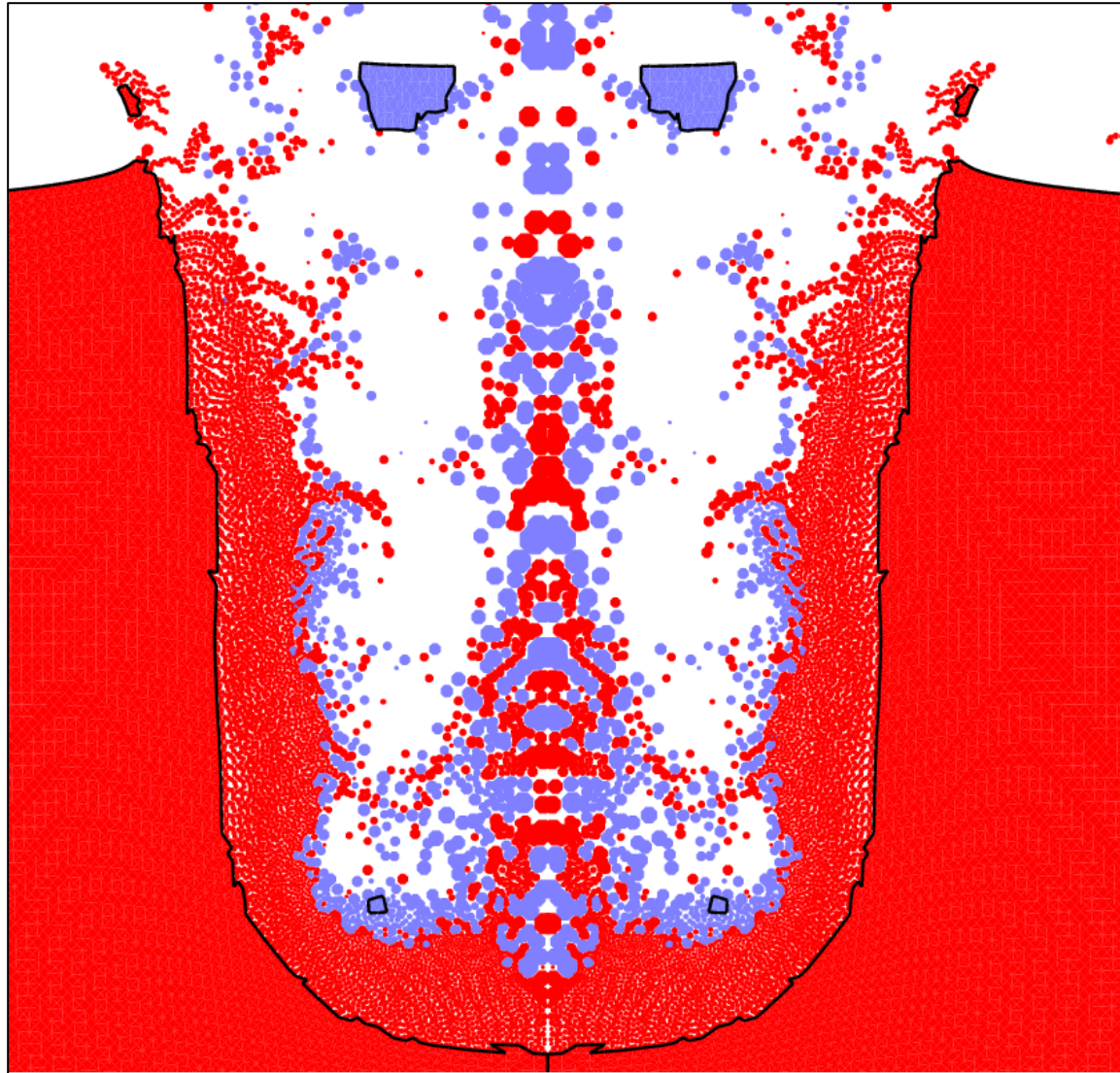
Figure 4.12 Fourth segment of alternate SRP design interacting with non-centralized ejecta plume
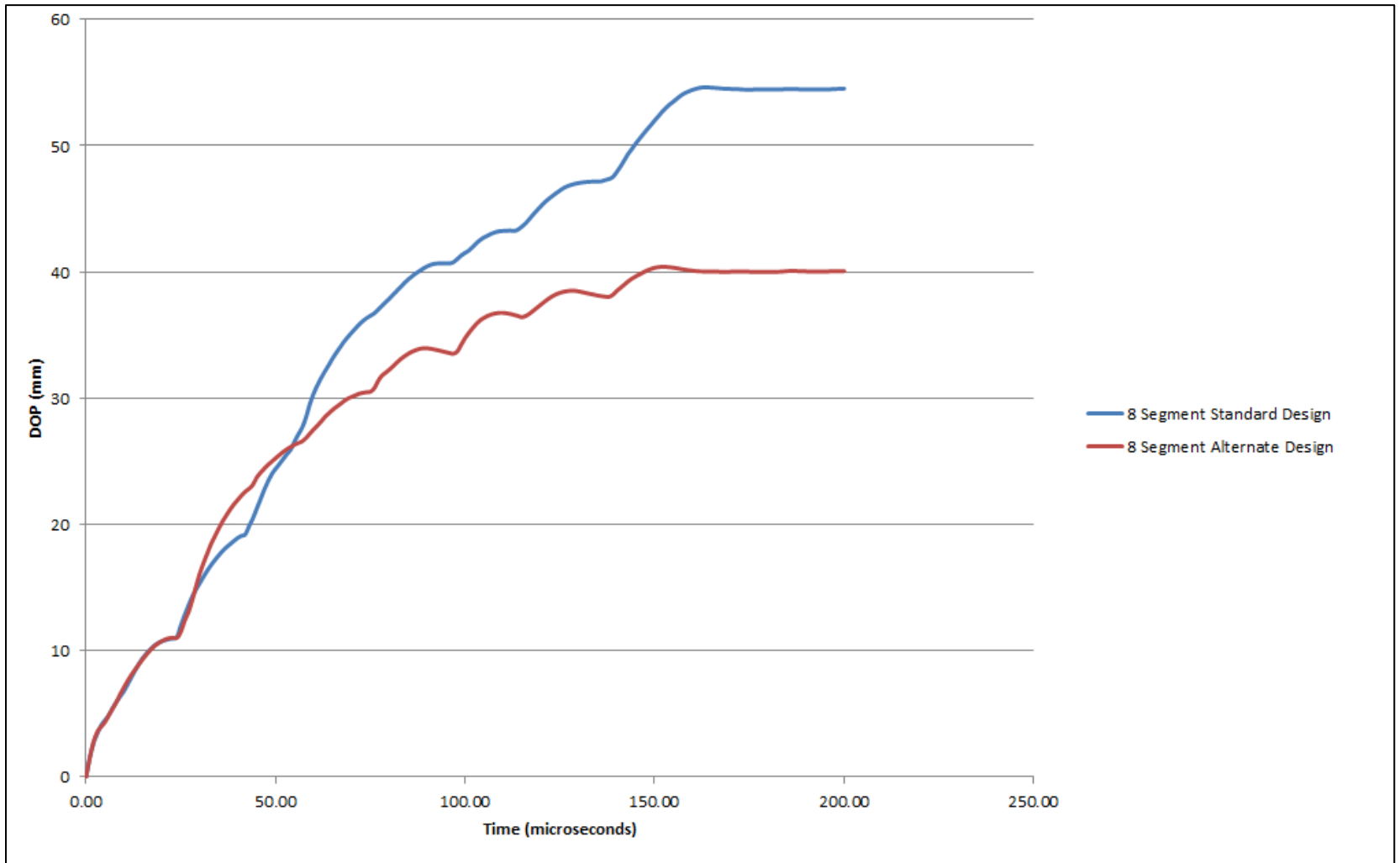
Figure 4.13. Depth of penetration comparison between all disc SRP and alternate washer SRP

Chapter 5

CONCLUSIONS & RECOMMENDATIONS

5.1 Conclusions

One of the ultimate goals of projectile design is obtaining optimum penetration performance by a projectile into thick targets. In general there are four main phases of penetration: 1) transient, 2) primary, 3) secondary, and 4) recovery. Mainstream kinetic energy projectiles penetrate thick targets during the "primary" penetration phase which is typified by a steady-state process. The basic concept behind segmented rod projectiles is that the initial transient penetration phase, typified by high transient shock stresses, is repeated over and over. Very little penetration by segmented rod projectiles is performed in a steady state regime. It is because of this repeated transient stress that experiments and simulations have proven that SRPs provide greater penetration efficiency. For a given mass of the projectile, the final DOP in the target seems to be influenced by the segment's aspect ratio, number of segments, spacing between the segments, and impact velocity.

The present work considered modeling and simulation of a heavy alloy tungsten projectile penetration into thick steel targets at very high velocities. The baseline velocity considered for this purpose was 2.6 km/sec. The 2006 version of the Lagrangian finite element software EPIC was employed for simulating a variety of penetration configurations. Since the DOP (depth of penetration) results were influenced by the various element erosion options available in EPIC, initially a sensitivity study was performed to establish a suitable erosion option for modeling the SRP problem. Based on this study, the element-to-particle conversion algorithm in EPIC which produced consistent DOP results was chosen in all simulations. To further validate the EPIC code results, a comparison study between this advanced Department of Defense penetration code (EPIC) with a commercially available Eulerian finite element software (AUTODYN). Though these two codes produced quantitatively different results, the DOP results did agree with respect to increased efficiency by SRP as compared to a monolithic long rod. Comparisons between the two codes were complicated by a lack of robust method to determine DOP in EPIC simulations. In addition, the simulation results from 2006 version of the EPIC code compared the effects of variety of design parameters and projectile configurations on penetration depths.

As other researchers reported that the penetration efficiency of a SRP is significantly greater than a single rod with same mass, the current high resolution EPIC simulations further confirmed the increased penetration efficiency by about 25% (see figure 4.6). However, an optimal spacing between the various segments needs to be estimated to obtain the best performance by a SRP. A comparison was performed between three different impact velocities: 1500m/s, 2250m/s, and 2600m/s. Based on computational results, a unique optimal spacing for each velocity is confirmed.

During the course of the penetration process, the tungsten penetrator dissolves into meshless particles. These particles are products of an element-to-particle conversion algorithm to handle excessive erosion of materials due large scale plastic deformation. Some particles embed in the crater walls but others form a focused ejecta jet that flow directly into the path of the incoming projectile segments. To understand the effects of ejecta on diminishing the full potential of the SRP concept, several EPIC simulations were performed with just by modeling two-segment SRP penetration into a thick steel target. It was observed that, during the first three segment impacts, this ejecta tended to flow in a coherent jet which was centralized along the axis of symmetry. An alternative design for an SRP was considered to accommodate this centralized plume by creating a hole in the center of the segment, thereby allowing the ejecta to flow through less impeded; this perhaps could enable the incoming segments to be intact for a longer period of time. Five different configurations were considered in EPIC simulations to evaluate the performance of the new alternate design with different hole diameters. DOP increased during the impact of the first three segments, but overall DOP for the alternate SRP design was 25% less than that of the standard SRP design. This decrease was likely due to the decentralization of the ejecta plume that destroyed the optimal shock and penetration loading conditions.

Based on these results, it was concluded that solid segments were far more efficient than "washer" type segments. Indeed, the idea of a new configuration to accommodate the ejecta flow by removing mass from the center portion of a solid segment and adding this removed mass to increase the thickness of that segment did not improve the penetration efficiency any further. On the contrary, the washer type segment showed reduced penetration due to the absence of mass in the center. In summary, the EPIC results reasonably established that an 8-segment SRP configuration was more efficient than a single long rod at high velocity impact.

5.2 Recommendations

The current work dealt entirely with two dimensional axisymmetric simulations. Three dimensional runs are needed in order to verify that the ejecta phenomenon observed is not an artifact of the two dimensional simulation. Once similar backflowing ejecta is demonstrated in three dimensional simulations, experiments with high speed photography are needed to verify the existence and character of the ejecta plume. If experimentally detected, new means of dealing with the ejecta problem can be developed.

BIBLIOGRAPHY

1. Tate, A. "Engineering modeling of some aspects of segmented rod penetrators". *International Journal of Impact Engineering 9.* 1990. pgs 327-341.

2. C.E. Anderson and J.D. Walker, "An Examination of Long Rod Penetration," Int. Journal of Impact Engineering, 4, pp. 481-501, 1991.

3. C.E. Anderson, B.L. Morris, and D. Littlefield, "A Penetration Mechanics Database," SWRI Report 3593/001, Jan 1992.

4. A.M. Rajendran, "Penetration of Tungsten Alloy Rods into Shallow-Cavity Steel Targets, Int. Journal of Impact Engineering, 6, pp. 451-460, 1998.

5. Zukas, Jonas A. *Impact Dynamics*. New York: Wiley, 1982. Print.

6. EPIC Code (2006 Version), Lead Developer: Dr. Gordon Johnson, Southwest Research Institute, Minneapolis, MN.

7. Normandia, Michael J. and Lee, Minhyung. "Penetration performance of multiple segmented rods at 2.6 km/s." *International Journal of Impact Engineering 23.* 1999. pgs 675-686.

8. ANSYS AUTODYN (old version)

9. M.J. Forestall and V.K. Luk, "Dynamic Spherical Cavity Expansion in a Compressible Elastic-Plastic Solid," Trans. ASME, J. Appl. Mech., pp. 275-279, 1988.

10. C.E. Anderson, Jr., and S.R. Bodner, "Ballistic Impact: The Status of Analytical and Numerical Modeling," Int. Journal of Impact Engineering, 7 (1), pp. 9-35, 1988.

11. Eichelberger, R.J. "Experimental Test of the Theory of Penetration by Metallic Jets." *Journal of Applied Physics*. 1956. Vol. 7. Pp 63-68.

12. Herbette, G. "The Influence of Projectile Shape on Penetration Power." Proceedings of the 11th International Symposium on Ballistics. 1989. pp561-567.

13. De Rosset, W.S. "Multilple Impacts on Monolithic Steel." Proceedings of the 6th International Symposium on Ballistics. 1981. Pp312-321.

14. Scheffler, D. R. "Two-Dimensional Computer Simulations of Segmented Penetrators." Technical Report BR-TR-3013. Ballistic Research Laboratory, Aberdeen Proving Ground, MD.

15. Cuadros, J.H. "Monolithic and segmented projectile penetration experiments in the 2 to 4 km/s impact velocity regime". *International Journal of Impact Engineering 10.* 1990. pgs 147-157.

16. Franzen, R.R., Walker, J.D., Orphal, D.L., and Anderson, Jr., C.E. "An upper limit for the penetration performance of segmented rods with segment-L/D $\leq$ 1". *International Journal of Impact Engineering 15* 1994. pgs 661-668.

17. Naz, P. and Lehr, H.F. "The crater formation due to segmented rod penetrators". *International Journal of Impact Engineering 10.* 1990. pgs 413-425.

18. Holland, P.M., Gordon, J.T., Menna, T.L., and Charters, A.C. "Hydrocode results for the penetration of continuous, segmented, and hybrid rods compared with ballistic experiments". *International Journal of Impact Engineering 10* 1990. pgs 241-250.

19. Kivity, Y., Yitzhah, E., Hirsh, E. "Segmented Rods into Homogeneous Targets." Proceedings of the 11th International Symposium on Ballistics. 1989. Pp473-479

20. Hohler, V. and Stilp, J. "Penetration performance of segmented rods at different spacing comparison with homogeneous rods at 2.5 – 3.5 km/s". Proceedings of the 12th International Symposium on Ballistics. 1990. pp178-187

21. Orphal, D.L, Anderson, C.E, Jr., Franzen, R.R., Walker, J.D., Schneidewind, P.N., and Majerus, M.E. "Impact and Penetration by L/D ≤ 1 Projectiles." *International Journal of Impact Engineering 14.* 1993. pgs 551-560.

22. Bjerke, T.W., Zukas, J.A., and Kimsey, K.D. "Penetration Performance of Disk Shaped Penetrators." *International Journal of Impact Engineering 12.* 1992. pgs 263-280.

23. Weihrauch, G. and Wollmann, E. "Segmented penetrators". *Propellants, Explosives, Pyrotechnics.* 1993. pgs 270-274.

24. de Rosset, W.S and Kimsey, K.D. "Calculation of Multiple Copper Rod Impacts on Steel Targets." Proceedings of the 9th International Symposium on Ballistics. 1990. Pp375-380.

25. Sedgwick, R.T., Waddell, J.L., and Wilkinson, G.M. "High Velocity Long Rod Impact: Theory and Experiement." Proceedings of the 10th International Symposium on Ballistics. 1988.

26. Hunkler, R. "Numerical simulations of segmented rods." Proceedings of the 11th International Symposium on Ballistics. 1988. pp 465-474.

27. Charters, A.C and Menna, T.L. "Penetration Dynamics of Rods from Direct Ballistic Tests of Advanced Armor Components at 2-3 km/s." *International Journal of Impact Engineering 10.* 1990. pgs 93-106.

28. Walker, J.D. and Anderson, Jr, C.E. "A nonsteady-state model for penetration". *Proceedings of the 13th International Symposium on Ballistics.* 1990.

29. Y. Partom, C.E. Anderson, "Further Investigation of the Target Resistance Penetration Parameter R_t," Shock Compression of Condensed Matters – 1999, edited by M.D.

Furnish, L.C. Chhabildas, and R.S. Hixson, pp. 1129-1132, American Institute of Physics, 1999.

30. Tolman, J., Satapathy, S., Landen, D., Barnette, D., Subramanian, R., and Bless, S. "Penetration Mechanics of Long Segmented Rods". *Hypervelocity Impact Symposium, April 11-15, Freiburg, Germany.* 2010.

31. Zukas, Jonas A. *High Velocity Impact Dynamics.* New York: Wiley, 1990. Print.

32. Chou, P.C. and Toland, R.H. "Experimental Study of Multiple Interior Impacts". *Experimental Mechanics 17.* 1977. pg 201-206.

33. de Rosset, William S. "Multiple Impacts on Monolithic Steel". *Proceedings, International Symposium on Ballistics.* 1981.

34. Zerilli, F.J. and Armstrong, R.W. "Dislocation Mechanics Based Constitutive Equation Incorporation Dynamic Recovery and Applied to Thermomechanical Shear Instability." *Proceedings of the American Physical Society Topical Group on Shock Compression of Condensed Matter Conference.* 1997. pg 215-218.

35. Johnson, G.R. and Cook, W.H. "A Constitutive Model and Data for Metals Subjected to Large Straing, High Strain Rates and High Temperatures." *Proceedings of the 7th International Symposium on Ballistics.* The Hague, The Netherlands. 1983.

36. S.R. Bodner and Y. Partom, "Constitutive Equations for Elastic-Viscoplastic Strain-Hardening Materials," J. Appl. Mech., Trans. ASME, 42, 385-389, 1975.

37. S.R. Bodner and A. merzer, "Viscoplastic Constitutive Equations for Copper with Strain Rate History and Temperature Effects," ASME J. Engg Mat. Tech., 100, pg 388-394, 1978.

VITA

1. Bachelor of Science Mechanical Engineering. May 2008. The University of Mississippi.
   University, MS 38677.

2. Graduate Research Assistant. August 2009- May 2012. The University of Mississippi.
   University, MS 38677.

3. "A Computational Study of Segmented Tungsten Rod Penetration into a Thick Steel
   Target Plate at High Velocities." Presented at the 17th Biennial International Conference
   of the American Physical Society Topical Group on Shock Compression in Condensed
   Matter. 26 June 2011-1 July 2011. Chicago, IL.